



RESEARCH ARTICLE

10.1029/2024JD041243

Key Points:

- Urbanization correlates with the presence of shallow cumulus clouds
- Urban clouds are driven by the enhanced sensible heat and dynamic drag imparted by the urban landscape
- Urbanization cloud enhancement emerges as a crucial pathway responsible for reducing the afternoon Heat Index values

Supporting Information:

Supporting Information may be found in the online version of this article.

Correspondence to:

J. F. Mejia,
john.mejia@dri.edu

Citation:

Mejia, J. F., Henao, J. J., & Eslami, E. (2024). Role of clouds in the Urban Heat Island and extreme heat: Houston-Galveston metropolitan area case. *Journal of Geophysical Research: Atmospheres*, 129, e2024JD041243. <https://doi.org/10.1029/2024JD041243>

Received 5 APR 2024

Accepted 23 AUG 2024

Author Contributions:

Conceptualization: John F. Mejia
Data curation: John F. Mejia, Juan Jose Henao
Formal analysis: John F. Mejia
Funding acquisition: John F. Mejia
Investigation: John F. Mejia, Juan Jose Henao, Ebrahim Eslami
Methodology: John F. Mejia, Juan Jose Henao, Ebrahim Eslami
Project administration: John F. Mejia
Resources: John F. Mejia, Ebrahim Eslami
Software: John F. Mejia, Juan Jose Henao
Supervision: John F. Mejia
Validation: John F. Mejia, Juan Jose Henao, Ebrahim Eslami
Visualization: John F. Mejia
Writing – original draft: John F. Mejia

© 2024, The Author(s).

This is an open access article under the terms of the Creative Commons Attribution-NonCommercial-NoDerivs License, which permits use and distribution in any medium, provided the original work is properly cited, the use is non-commercial and no modifications or adaptations are made.

Role of Clouds in the Urban Heat Island and Extreme Heat: Houston-Galveston Metropolitan Area Case

John F. Mejia¹ , Juan Jose Henao¹ , and Ebrahim Eslami² 

¹Division of Atmospheric Sciences, Desert Research Institute, Reno, NV, USA, ²Houston Advance Research Center, The Woodlands, TX, USA

Abstract This study examines the influence of shallow cumulus clouds on the excessive summertime heat in the Houston-Galveston metropolitan area, a coastal urban area in the warm Southeast United States. Specifically, it aims to improve our understanding of how both the clouds and the relatively cool, moist afternoon sea breeze impact the Urban Heat Island (UHI) and Heat Index (HI). During the warm season, the afternoon sea breeze phenomenon in this coastal city acts as a natural air conditioner for city residents, facilitating the dispersion of moisture, heat, and pollutants. To investigate the relationship among urbanization, clouds, and land-sea interactions, we conducted cloud- and urban-resolving simulations at a 900 m grid resolution and perform simulation scenarios aiming to isolate urbanization, clouds and land-sea circulations. Results show that urbanization correlates with the presence of shallow cumulus clouds, higher cloud bases, and increased cloud duration over the Galveston-Houston region compared to rural areas. These urban clouds benefit from the enhanced moist static energy that is favored by intensifying vertical mixing and moisture flux convergence. Urbanization raises the mean HI while mitigating its afternoon HI high. We found that the urban circulation dome overwhelms the sensitivity of the sea breeze to the urbanization. Instead, the influence of urbanization on cloud enhancement emerges as a crucial pathway responsible for reducing the high afternoon HI values. Moreover, uncertainties in SSTs are closely linked to the sensitivities of land-sea circulations, which in turn modulate UHI and HI.

Plain Language Summary Urbanization influences the meteorology by creating a warmer environment that enhances excessive heat during the summer. Additionally, the warmer environment and the urban buildings increase friction, leading to more mixing and in turn favoring the development of low-level clouds. We developed computer simulations aiming to understand these processes and their interaction with the sea-breeze in this coastal city, and we found that these clouds help ameliorate the excessive heat during the afternoon.

1. Introduction

This study is motivated by the need to characterize and better simulate excessive heat in urban environments. Increasing population in urban areas make cities more vulnerable to extreme weather events, climate variations and warming trends. It is likely that some of these changes will be outside of the range of historical extremes (Simolo et al., 2011; Trenberth et al., 2015) and are expected to cause changes not only in mean, but also in extreme weather episodes (USGCRP, 2018). While there is relatively high confidence in the direction of changes in extreme temperature episodes, decision-makers require more quantitative and detail information to make better and more concrete adaptation plans to improve resilience in natural resources management (Rosenzweig et al., 2014) and health related risks (Ebi et al., 2021; Guo et al., 2018). The exposure of cities to extreme heat appears to be more critical under climate change scenarios and is exacerbated by the high solar absorption of the urban environments (i.e., the Urban Heat Island (UHI) effect, hereafter UHI) (Fischer & Schär, 2010; Schubert et al., 2012). Hence, understanding the processes modulating the extreme temperature is a necessary step to develop reliable adaptation and mitigation strategies aiming to make cities more resilient (Cady et al., 2020; Houston Climate Action Plan, 2020; Resilient Houston 2020; Zonato et al., 2021).

Several studies have found that the urban environments not only modulate the temperature via the UHI effect, but also other weather parameters such as local circulation (Banks et al., 2015; Kim et al., 2013; Spangler & Dirks, 1974) and clouds and precipitation (Changnon et al., 1971; Doan et al., 2023; Fan et al., 2020; Loughner et al., 2011; Moraglia et al., 2024; Statkewicz & Rappenglueck, 2023; Theeuwes et al., 2019; Vo et al., 2023).

Writing – review & editing: John F. Mejia, Juan Jose Henao

During the daytime, observations (Banks et al., 2015; Spangler & Dirks, 1974; Theeuwes et al., 2019), long-term satellite clouds retrievals (Vo et al., 2023) and numerical simulations (Fan et al., 2020; Loughner et al., 2011; Moraglia et al., 2024; Theeuwes et al., 2021) have shown that the urban environment favors a deeper mixing layer and enhances warm non-precipitating clouds (i.e., low-level shallow cumulus clouds); cities can also enhance extreme precipitation (Doan et al., 2023; Fan et al., 2020). During the night, however, Vo et al. (2023) suggested that clouds can block outgoing longwave radiation and exacerbate the UHI by suppressing the nighttime cooling.

The role of the urban environment on simulated warm non-precipitating low-level clouds needs a more systematic and deeper assessment as it can be influenced by the geography and climate of the region (Chiu et al., 2022; Theeuwes et al., 2021; Vo et al., 2023). For example, Vo et al. (2023) observed that urbanization in cities near the Gulf Coast tend to show larger cloud enhancements during the summer, compared to other regions in the continental United States. For a single storm event, Fan et al. (2020) simulated the individual and combined effects of the urban land-use/land-cover and aerosols on convective clouds, storm evolution and intensity. In agreement with Theeuwes et al. (2019, 2021), Fan et al. (2020) showed that Houston urban area is also related to earlier occurring and more persistent clouds due to a stronger urban heating. They also showed that the aerosol-cloud interaction effect can develop deeper convective mixed-phase clouds and more intense storms as compared to the effect of the urban land-use/land-cover alone.

These cloud and precipitation enhancement favored by urbanization can modulate the UHI and extreme heat indicators. It is possible that the enhanced daytime clouds serve as a self-cooling mechanism by blocking the incoming solar radiation and increasing evaporative cooling. In coastal cities, however, isolating the effect of urbanization is challenging because the land-ocean sea breeze circulations can also invigorate clouds and precipitation (Loughner et al., 2011; Zhong et al., 2017) and overwhelm the signals related to urbanization, and other important processes such as aerosol-cloud interactions (Fan et al., 2020). During the extreme warm season, on the other hand, the relatively cold and moist air masses advected by the afternoon sea-breeze phenomenon provide a natural air conditioning to the city's residents, and facilitates the redistribution of pollutants, moisture, and heat.

The interaction between the urban heat and clouds remains poorly understood. Specifically, how does the interplay between Houston-Galveston urban morphology and local circulations influence the formation and behavior of clouds over the city? What are the specific dynamic and thermodynamic mechanisms driving the formation of urban-induced clouds in the urban area? What is the relationship between surface temperature and humidity, urban heat, and the formation of urban-induced clouds? To address these questions, we conducted urban-resolving and cloud-resolving simulations (900 m grid size) using the Weather and Research Forecasting model (WRF; Powers et al., 2017). Incorporating a multilayer urban canopy model (UCM) focused over the Houston-Galveston area, our simulations leverage state-of-the-art representations of urban morphology and Local Climate Zones (LCZ) (Demuzere, Kittner, et al., 2022a; Demuzere et al., 2023). In Section 2, we describe the model configuration, outline the observational data used for model evaluation, and elucidate the rationale behind our experimental design, which aims to isolate the impacts of urbanization and coastal influences. Moving forward to Section 3, we present the evaluation results of our model, and examine the model representation of the UHI intensity, HI, and shallow cumulus clouds. Furthermore, we delve into the analysis of pertinent dynamical and thermodynamical processes within the mixed layer, as well as the intricate land-sea interactions that drive cloud enhancement. Finally, Section 5 offers a comprehensive discussion, reconciling new findings and drawing conclusive insights from our study.

2. Data and Methodology

2.1. The Regional Climate Model Coupled With the Urban Canopy Model

We used the Weather Research and Forecasting model (WRFv4.3.2; Powers et al., 2017) to perform urban- and cloud-resolving simulations. For this, we implemented the UCM based on the multi-layer building effect parameterization (BEP) scheme, coupled with the Building Energy Model (BEM; Salamanca et al., 2011). This UCM option considers three-dimensional mass and momentum mixing and heat transfer between buildings and the atmosphere, providing a realistic and accurate representation of near-surface energy fluxes and air temperature in mid-latitude cities (Cady et al., 2020; Jin et al., 2021). We would like to stress that this is not an instance of model calibration, but an attempt to assess and understand the UCM's capabilities and related uncertainties. We used this UCM option, among others available, because it incorporates 11 LCZ, with 10 built up categories that

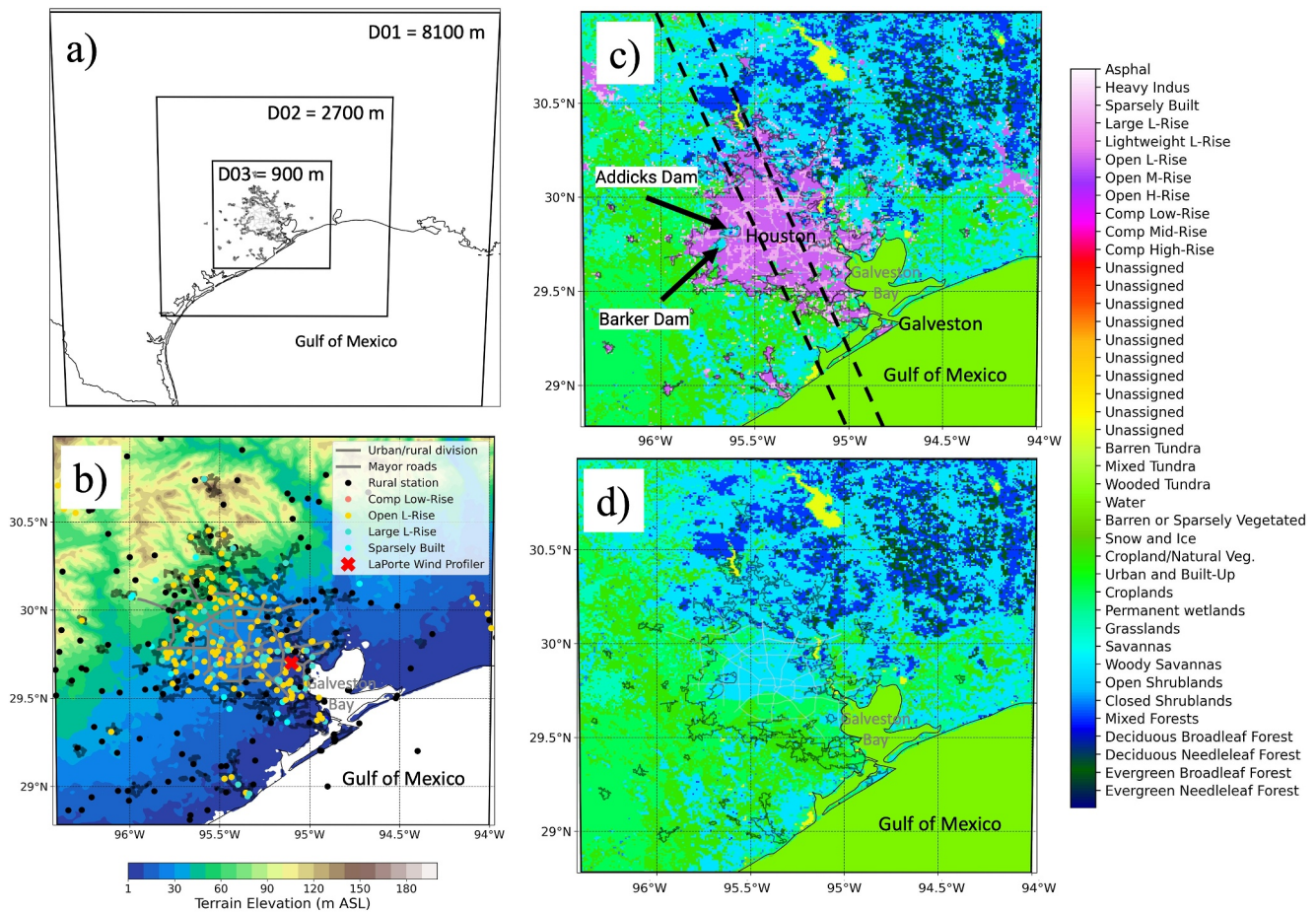


Figure 1. (a) WRF model nested domains (8,000, 2,700, 900 m grid sizes) and (b)–(d) details of the innermost model domain: (b) terrain elevation and the location of the NOAA LaPorte wind profiler site and the surface stations used in the model evaluation (from various sources), categorized by urban Local Climate Zones (LCZ; color coded symbols; 151 sites) or rural land cover (black symbols; 91 sites); (c) Land Use/Land Cover (LULC; contours) based on Demuzere et al. (2022a) using LCZ categories for the urban areas and MODIS for rural areas; and (d) LULC after removing the urban areas and replacing them with the surrounding predominant rural vegetation. Dark gray contours indicate urbanization boundaries as of 2010 (Houston-Galveston Area Council, H-GAC; <https://www.h-gac.com/Home>) and light gray polygons show location of major intraurban roads. Dash lines in panel (c) show the location of the cross-city transect shown in the analysis.

provide a more detailed representation of the heterogeneity of urban areas as compared to the three built-up categories in other databases and UCMs.

In this study, we used a three nested domain configuration (8,100 m, 2,700 m, and 900 m) centered in Houston, with 61 vertical levels up to 100 hPa (Figure 1). To allow the innermost model domain to relax toward the scenario settings, we designed the borders to be at least 80 km away from the suburban areas of Houston. Our initial modeling tests showed significant numerical diffusion noise, highlighted as non-physical wind street patterns and thermal fields in the mixing layer with a spatial scale of two times the grid size. This problem is relatively common in high-resolution simulations during weak wind conditions and weak or unstable stratification (Crosman & Horel, 2012; Knievel et al., 2007). To overcome this issue, we imposed a spatial filter based on an explicit sixth-order numerical diffusion scheme with a non-dimensional rate of 0.12. Despite the potential over smoothing in space of surface processes, the explicit diffusion treatment notably improved simulations, and results were resistant and unsensitive to its implementation. Additionally, we combined our experience and literature reports to determine other configurations and the selection of physical parameterizations implemented in our model. We acknowledge that it is difficult to find a model configuration that is superior under different flow regimes and for the large variety of geography and urbanization settings. For parameterization of moist processes, we used the Thompson double-moment microphysics, whereas convection and clouds parameterization are resolved explicitly in all our model domains, except for the coarser grid (8,100 m) where we used the Kain–

Fritsch scheme. Additionally, we used the Dudhia and Rapid Radiative Transfer Model as shortwave and longwave radiation schemes, respectively; Noah-Multiparameterization, Monin-Obukhov and Yonsei University (YSU) were selected for land-surface model, surface layer, and planetary boundary layer (PBL) schemes, respectively. YSU PBL scheme was used for its simplicity, low computational cost and recognized good performance (Hendricks et al., 2020). The first 6 hr of the simulations were not considered to allow for the model spin up. We used the GDAS/FNL (the Global Data Administration System/Final) re-analysis data set (National Centers for Environmental Prediction et al., 2015; hereafter “FNL”) as initial and boundary conditions data, with Sea Surface Temperature (SST) skin temperature updated as bottom boundary condition SSTs every 6 hr.

2.2. Land Use/Land Cover and Urban Characterization

An important consideration in urban canopy modeling is the characterization of the Land Use/Land Cover (LULC) and urban categories. Most LULC products rely on remote sensing surveys with urban classification that are either outdated, such as the National Urban Database and Portal Tool (NUDAPT; Ching et al., 2009), or lack details even in major urban composition features, such as the World Urban Database and Access Portal Tools version 2 (WUDAPT; Brousse et al., 2016; Ching et al., 2018; Demuzere et al., 2021, 2022a). Additionally, differences in the algorithms used to characterize urban categories and different data sources may result in different urban coverage. We opted to implement the 100 m global map of LCZ (Demuzere et al., 2023) for the following considerations: (a) it follows the WUDAPT protocol; (b) it is based on more modern (2016–2018) data than NUDAPT, thus it captures a more recent snapshot of the urban growth and with a better spatial resolution; and (c) their land cover classification is adapted to the 11 LCZ, contrasting only three urban categories in the NUDAPT data. Recently, the global LCZ map was introduced into WRF preprocessing system (Demuzere et al., 2023). However, we did not implement this version as the LCZ rely on urban pixels from other databases (MODIS and Copernicus), producing a smaller urban area in comparison to the original global LCZ map for the study region. The preprocessing for WRF was performed using the WUDAPT-to-WRF (W2W) python tool (Demuzere, Argüeso, et al., 2022).

2.3. Model Experiment Design

All simulations cover a 15-day period, between August 1 and 16, 2020, which was the warmest period of 2020, and normally the warmest period of the year (Palecki et al., 2021). We excluded the initial 6 hr due to model spin-up issues. During the simulation period, however, different meteorological regimes could have modulated sea-breeze related convection invigoration: a pre-trough regime (1–3 August), followed by a post-trough regime (4–5 August), and then the Bermuda high anticyclone was more pronounced (5–16 August) (Wang et al., 2022; <https://earth.nullschool.net/>). To isolate the effect of these intermittent and scattered summer showers (mostly concentrated during August 1–3), we constrained our analyses to times without significant observed precipitation events (<5 mm) in the Houston-Galveston area.

2.3.1. SST Sensitivity

The city's proximity to the Gulf of Mexico and the complex coastal shape of Galveston Bay warrants a careful look at the SST data used by the model as bottom boundary conditions (Hawbecker & Knievel, 2022). When comparing the default FNL SST fields used by the model against measurements from remotely sensed NOAA-SNPP Visible Infrared Imaging Radiometer Suite (VIIRS) SST (available daily at 4 km grid size; several snapshots per day; Bouali & Ignatov, 2014) and buoy data sets (<https://www.ndbc.noaa.gov/>), we found an average offshore cold bias of nearly -1°C (Figure S1 in Supporting Information S1). To improve the SST fields, we implemented a time-space Barnes interpolation approach with successive correction using a Gaussian weight function departing from the untreated FNL SSTs until optimizing the agreement between the interpolated function and the measurements (the unbiased SSTs; Figure S1 in Supporting Information S1).

2.3.2. Clouds, Urbanization and Weather Sensitivity

We conducted a series of simulations to elucidate the intricate interplay between synoptic, sea-breeze, and cloud effects alongside urbanization's influence on meteorology.

First, we established a Baseline simulation incorporating the LCZ categories to mimic the urban landscape, using the unbiased SST as bottom boundary conditions (as outlined in Section 2.3.1), along with cloud and precipitation

physics representations (microphysics and convection). Clouds and showers, partly driven by the afternoon sea-breeze, can significantly impact the UHI effect (Morris et al., 2001). However, given the relatively short duration of our simulations (15 days) and the sporadic nature of moist processes aloft, we executed a clear sky simulation (hereafter referred to as “Clear sky”) by deactivating microphysics and convection in the model. This method assists in partially isolating the impact of clouds and showers on the UHI effect. However, fully disentangling the role of clouds in the UHI presents a challenge due to their potential influence on mesoscale circulations, such as sea breezes and urban-rural thermal-related flows, which are known to also affect the UHI phenomenon.

To assess uncertainties associated with SSTs, we performed a simulation utilizing the original (untreated or biased) FNL SSTs fields (hereafter referred to as “Biased SSTs”). Additionally, we isolated the urbanization effects within mesoscale circulations by eliminating all urban areas from the domains (hereafter referred to as “No City”), replacing all urban grid points with representative regional vegetation (Figure 1d). A summary of the simulations conducted in this study, along with their respective descriptions and justifications, is provided in Table 1. Of note is that all references to the model simulation pertain to the Baseline scenario, unless explicitly stated otherwise.

2.4. Surface Station and Upper-Air Winds

We utilized all available, quality-controlled surface station monitoring sites in the Houston area and surrounding rural regions. Data was retrieved using the Synoptic Data Application Programming Interface (API) using data from the National Weather Service, Remote Automated Weather Station, and Texas Commission on Environmental Quality (TCEQ) Continuous Ambient Monitoring Station (CAMS) network. After stringent quality assurance/quality control checks (e.g., removing outliers, visual inspection, addressing atypical diurnal cycles of temperature and relative humidity), a total of 242 stations were deemed reliable for our analyses, with 151 situated in urban settings (110 in Open L-Rise, 12 Sparsely built, 28 in Large L-Rise, and 1 in Open H-Rise) and 91 in rural areas (Figure 1b). It is acknowledged that certain uncertainties may exist due to urban network siting and sensor variability (Qian et al., 2022), some of which were mainly designed for air quality monitoring purposes (e.g., TCEQ sites).

These surface station observations significantly contributed to assessing the model confidence in representing the diurnal temperature, relative humidity, and wind behavior, while facilitating the analysis of derived parameters such as minimum and maximum temperature (T_{\min} and T_{\max}), UHI, and HI, based on the Rothfusz (1990) formulation utilizing temperature and relative humidity data. We estimated UHI as the temperature differences between mean Urban minus Rural sites during local T_{\min} and T_{\max} times. A potential uncertainty in our approach to estimate UHI could originate from the differences in time of occurrence of T_{\min} and T_{\max} between urban and rural sites. We assessed the time of occurrences, and the time differences are only within 1 hour. We estimated UHI using the same time from both rural and urban yielding unsignificant differences when compared to our local time approach (not shown). Model confidence was assessed through metrics including model bias, root-mean-square-error (RMSE), and Pearson correlation coefficient. In order to enable a comprehensive comparison between urban and rural sites, we employed a bootstrapping methodology with replacement. This approach was designed to assess the uncertainty surrounding the impact of proximity to the coast and the consequent land-sea interaction effects; the distance from the coast (i.e., from the station to the nearest simulated ocean grid point) can also have an impact in the UHI estimates (not shown). Specifically, we used the median of the distance from the coast to subsample and balance the number of sites located near the coast with those far from the coast. The bootstrapped analysis included an almost equal distribution of stations between coastal and inland locations relative to downtown Houston, situated approximately 75 km from the Gulf coast. Consequently, coastal sites were classified as being within a coastal area if their distance from the Gulf coast was less than 75 km, while inland sites were those located further away.

To assess the accuracy of simulated low-level winds, we compared them against observations from the Cooperative Agency Profilers wind profiler at La Porte (LPTTX), situated near the coast along the northern shores of Galveston Bay (Figure 1b).

3. Results

3.1. Model Evaluation

Figure 2 shows the observed and simulated diurnal patterns of surface temperature, relative humidity, HI, and zonal and meridional winds, corresponding to urban and rural sites in the domain. In general, the model

Table 1*Description of Model Scenarios Simulated in for This Study*

Scenario name	Description	Justification
Baseline	All sky simulation including cloud and convective processes (moist processes) and bias correction of offshore SSTs (unbiased SSTs). Includes WUDAPT data.	Full physics simulation using outlined parameterizations and state-of-the-art LULC categories from LCZ. Systematic biases associated with offshore SSTs are removed.
Clear sky	Same as Baseline but without clouds and moist convective processes.	Isolate the role of clouds and precipitation relative to Baseline.
Biased SST	Same as Baseline but using the untreated biased SSTs	Assess the sensitivity of Baseline to SST perturbations or refinements (e.g., bias corrections).
No city	Same as Baseline but replacing the urban LCZ categories with rural land cover	Isolate the role of the urbanization in the meteorology.

adequately follows the diurnal median patterns for the evaluated parameters, but several biases are apparent, with the model showing a systematic low relative humidity bias (also exhibited in the water vapor mixing ratio, not shown) that is more intense during the afternoon and nighttime. The model surface temperature shows an in-phase diurnal evolution with a warm bias in the late afternoon and during the nighttime. Of note is that model nighttime temperature biases are even warmer in urban sites compared to rural sites, likely due to high urbanization-related outflux ground heat and sensible heating. The amplitude of the diurnal cycle of the simulated HI exhibits a smaller magnitude compared to observational estimates, characterized by a warm bias during nighttime and a cold bias during daytime periods. These biases in HI stem from a concurrent warm bias in surface temperature during the day and a dry bias in relative humidity during the night. Notably, these HI biases are more pronounced over urban sites, where the dry bias is more discernible.

Figure 2 shows that the diurnal distribution of the simulated zonal winds closely follows the observations, with shifting from relatively calm southeasterlies in the morning to stronger southwesterlies at 12:00 Local Time (Central Daylight Time; “LT” hereafter), with maximum at 17:00 LT, and extending during nighttime. Part of the wind shifting feature is typically a result from the PBL diurnal inertial oscillation (Blackadar, 1957); albeit diurnal variability at this region can also be driven by the sea-breeze circulation. Given the complex interaction between the vertical mixing, urban, and land-sea induced circulations, we extend these analyses aided by difference across simulations scenarios in Section 3.4. A striking surface circulation feature in Figure 2 is that wind speeds are stronger over rural areas compared to urban areas, likely due to the enhanced roughness and building barrier effects in urban sites (Li et al., 2021; Oliveira et al., 2003). This urban-rural wind speed differences are adequately simulated by the model, with some striking biases showing a slightly stronger southerly daytime wind bias in urban sites. In contrast, during late afternoon and overnight, the biases are more pronounced and almost doubles the observed southerly wind in rural sites.

To further assess the confidence in the simulated low-level wind patterns (<3 km), data from the La Porte wind profiler (Figure 3) were incorporated into our evaluation analysis. Both model simulations and observational data revealed a nocturnal wind acceleration, a phenomenon associated with the prevailing summertime Great Plains low-level Jet circulation, which extends toward the Gulf coast in eastern Texas (Pu & Dickinson, 2014). However, notable disparities emerged between the model and the observed conditions at La Porte. The model exhibited a more pronounced and enduring nocturnal maximum, suggesting a deeper intensity compared to the observed jet. This finding agrees with the results of Ngan et al. (2013), who identified analogous biases in model-generated low-level wind patterns and intensities across various land surface and PBL parameterizations. Additionally, the southerly wind bias feature resembles that of the surface wind biases, more strongly emphasized over rural sites. It is possible that stronger southerly winds are tied to the afternoon and nocturnal warm surface temperature biases outlined earlier. Remarkably, the No City scenario helps remove these biases (Figure 3d) suggesting this connection is plausible. Although it is out of the scope of this study, an energy and momentum budget can help elucidate and shed more light on the origin of the existing stronger southerly low-level wind biases.

Figure 4 shows the model scenarios biases (Table 1) for surface temperature and relative humidity, evaluated at all available surface station sites (see Figure S2 in Supporting Information S1 for evaluation of the RMSE and Pearson correlation coefficients). In general, model errors are small and well within the model typical behavior in

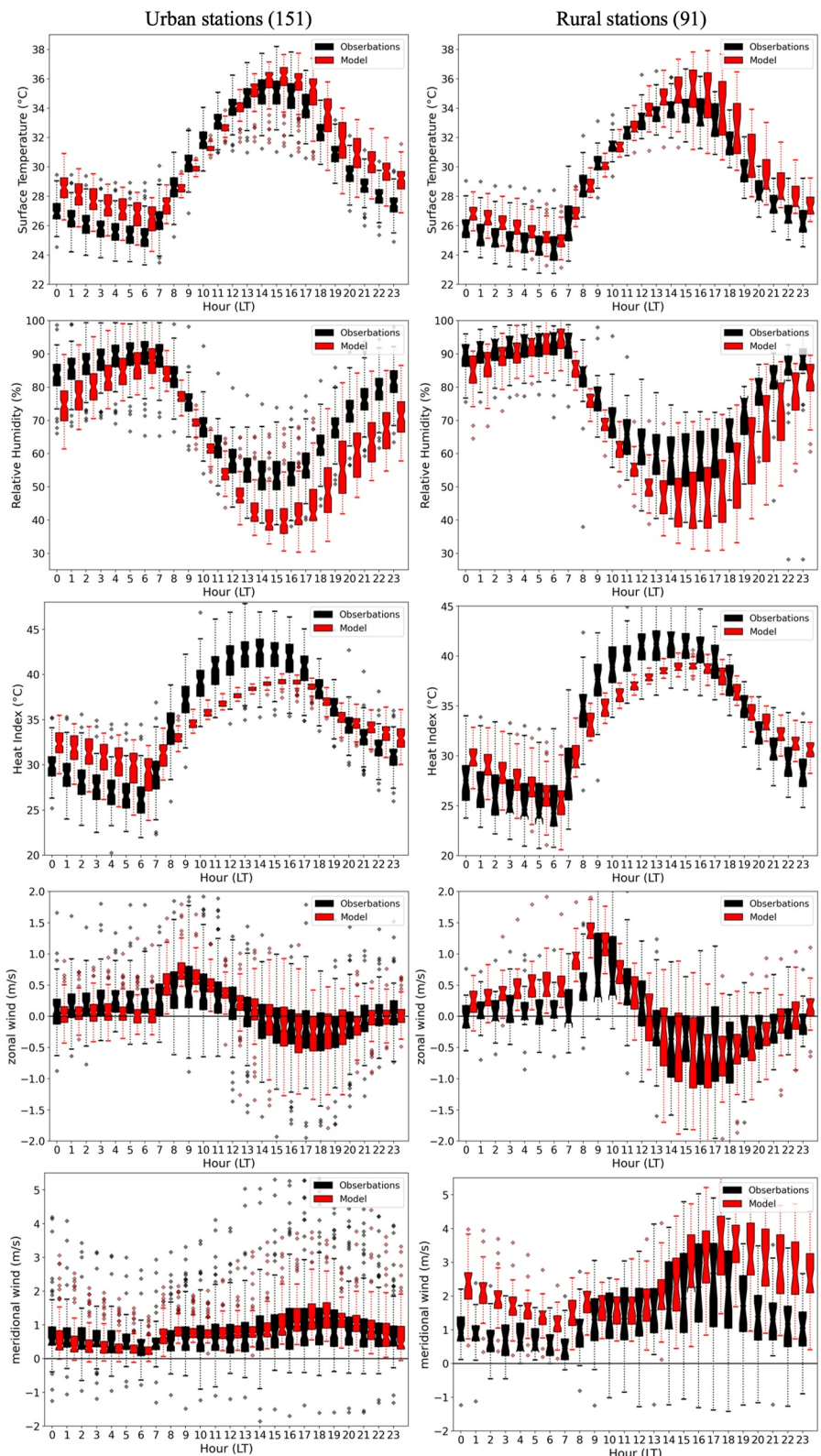


Figure 2. Baseline model and observed diurnal cycle distribution of (top to bottom panels) surface temperature, relative humidity, and zonal and meridional wind components for stations in the Houston urban (151 sites; left panels) and rural regions (91 sites; right panels).

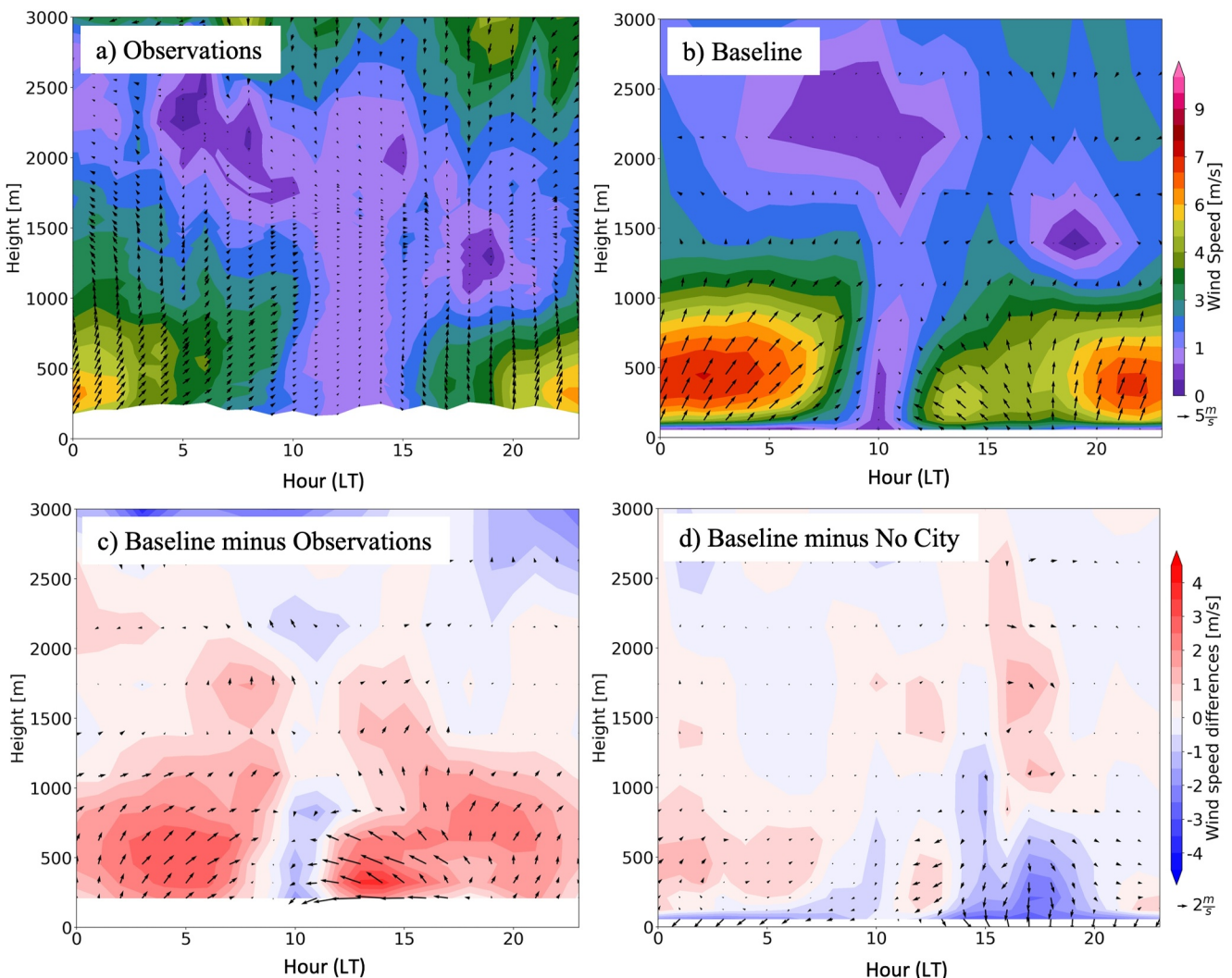


Figure 3. Low-level-diurnal mean horizontal wind speed (contours) and wind vectors (with the north direction pointing upwards) for (a) La Porte Wind profiler observations, (b) Baseline model winds, (c) Baseline minus observations differences, and (d) Baseline minus No City differences.

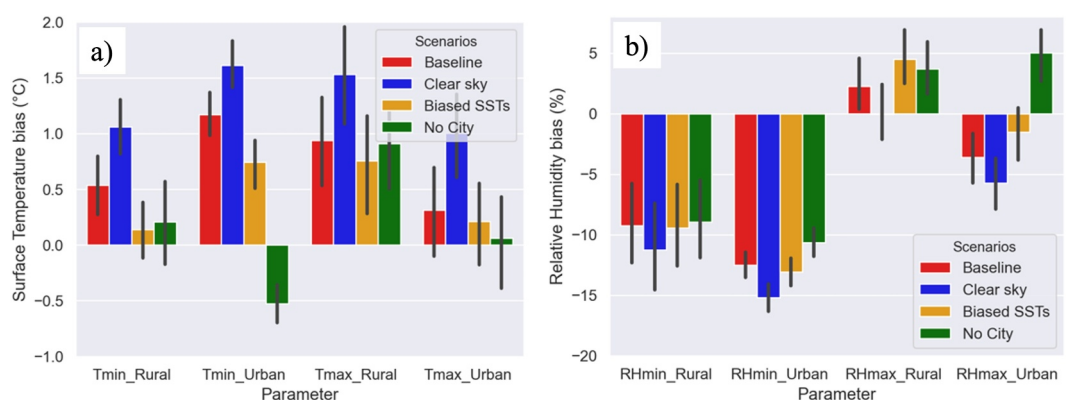


Figure 4. Model biases for each scenario (Table 1) evaluated at surface station sites for minimum and maximum (a) surface temperature and (b) relative humidity. Surface station sites are categorized as Urban or Rural according to land use/land cover types. Analysis is constrained to non-rainy periods as described in Section 2.

perturbed sensitivity experiments (Ancell et al., 2018; Wang et al., 2023), but some systematic error signals emerged as a function of the scenario simulations and by compositing rural and urban areas. The Baseline simulation shows a systematic warm bias for T_{\min} and T_{\max} . Not surprisingly and emphasizing the role of the UHI, over the urban areas the No City scenario shows a relatively colder bias when compared to all the urbanized scenarios.

The role of clouds in the model performance is apparent. Notably, the Clear sky scenario has warmer and drier biases during the daytime, as the lack of clouds increases the incoming solar radiation, balanced by more sensible and ground heating (Figure 4). At night, the warmer biases of the Clear sky scenario, as compared to Baseline biases, suggest that the outflux ground heating and high urban sensible heat flux, absorbed during the daytime due to increase shortwave radiation, dominate the faster Clear sky longwave radiation cooling (Figure 5). When comparing the Baseline to the Biased SSTs scenario, refining the offshore SSTs toward a warmer SSTs have an inland warming effect, with larger differences during early morning. Therein, a surprising result is that bias differences between Baseline and Biased SSTs are smaller during the daytime than during the early morning. This is related to the direct sea-breeze advection of warmer maritime surface temperature that does not develop a significant sensitivity in T_{\max} in comparison to T_{\min} . Below (Section 3.4), we show that the warmer SSTs in the Baseline simulation also promotes a weaker sea breeze that help further explain this reduced sensitivity. Therefore, the model biases highlight that the surface temperature sensitivity between the Baseline and Clear sky simulations (-0.56°C difference) are significantly larger than that between the Baseline and Biased simulations (0.25°C difference; see also Figure S2 in Supporting Information S1). By construction, the bias trends of the scenarios in this model evaluation procedure are somehow expected, but some potential non-linear impacts related to changes in cloudiness and circulation, which motivate the main objective of this study, are not as apparent.

3.2. Urban Heat Island

Table 2 compares surface station observations and corresponding simulations composited as a function of the rural and urban categories. The UHI was estimated as the difference between the mean temperature of the stations in the urban and rural sites, determined for T_{\max} and T_{\min} . Observations show a more pronounced UHI effect for T_{\max} (afternoon; averaging at 15:00 LT) than for T_{\min} (early morning; averaging at 06:00 LT). When contrasting the model at sites with surface station data, the Baseline model is overemphasizing the T_{\min} UHI effect and underemphasizing that of T_{\max} . To examine the role of clouds on the UHI, Table 2 shows that the Clear sky scenario is related to both stronger urban T_{\min} and T_{\max} , relative to Baseline. However, the resulting Clear sky UHI is milder than baseline at T_{\min} times, owing to enhanced surface longwave radiation cooling during the nighttime and enhanced shortwave radiation fluxes reaching the surface (not shown). Overall, the colder offshore Biased SST simulation shows colder mean temperatures over urban and rural areas, and during T_{\min} and T_{\max} times, but yields a similar and a more intense early morning and afternoon UHI, respectively. Finally, and by construction, the relatively small temperature differences in the No City simulation show that the composited UHI in the other simulations are linked to urbanization.

Another method to reveal the intensity of the UHI is by comparing the Baseline and the No City scenarios. Figure 6 shows the spatial patterns of the UHI effect for T_{\min} and T_{\max} , estimated as the Baseline minus the No City simulated differences. The nighttime and daytime UHI differences are striking, highlighting a very pronounced and significant early morning UHI effect and a less intense afternoon UHI effect (Figure 6c). The urbanization intensity and intra-urban vegetation islands are related to some of the cool UHI patches within the city (Figure 1c). Notably, the Baseline minus the No City differences remain significant downwind and to the north and northwest of the city boundary (Figure 6). Since some stations are located downwind of Houston, this advection of UHI can reduce the actual UHI intensity estimates shown in Table 2. Hence, the overemphasis of the early morning (T_{\min}) UHI can be partly attributed to the overestimation of surface temperature in the urban areas.

3.3. The Role of Shallow Cumulus Clouds

Figures 7a and 7b show the mean vertical maximum cloud mixing ratio for the Baseline and No City scenarios, respectively. The Baseline urbanized area exhibits thicker and more abundant clouds compared to the “urban area” in the No City scenario, primarily attributed to afternoon shallow cumulus clouds (Figure 7c). In contrast, the No City scenario shows a lower cloud cover with less apparent differences across the domain. The impact of

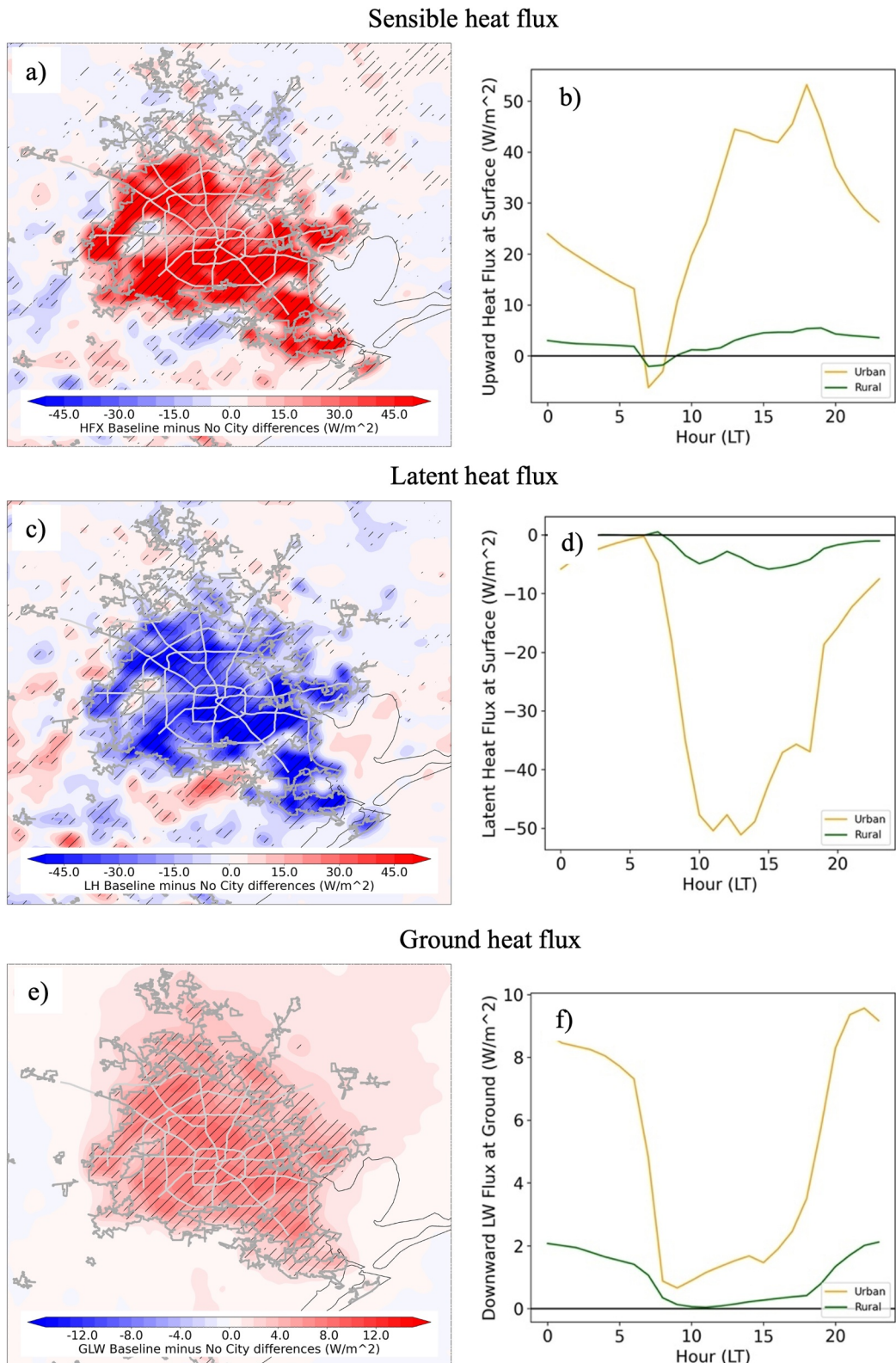


Figure 5. Mean Baseline minus No City differences for (a) sensible, (c) latent, (e) ground heat fluxes. Hatched areas indicate that differences are significant with a 95% confidence level. Dark gray contours indicate urbanization boundaries as of 2010 (Houston-Galveston Area Council, H-GAC; <https://www.h-gac.com/Home>) and light gray show location of major intraurban highways. Spatially averaged diurnal (b) sensible, (d) latent, and (f) ground heat fluxes for Baseline minus No City differences composited by urban and rural areas.

Table 2

Observed and Simulated (Mean and Bootstrapped 95% Confidence Interval Using for 100 Iterations With Replacement) T_{min} and T_{max} at Surface Station Locations Composed by Urban (151 Sites) Rural (91 Sites) Sites (See Figure 1)

	T_{min} [°C]				T_{max} [°C]				T_{min} [°C]		T_{max} [°C]	
	Rural mean	C.I. 95%	Urban mean	C.I. 95%	Rural mean	C.I. 95%	Urban mean	C.I. 95%	Mean	p-value	Mean	p-value
Observations	24.56	0.28	25.18	0.19	34.52	0.24	35.65	0.22	0.62	0.0002	1.13	<0.0001
Baseline	25.10	0.20	26.35	0.17	35.46	0.32	35.96	0.42	1.25	<0.0001	0.50	0.07
Clear sky- baseline	25.62	0.19	26.80	0.17	36.05	0.34	36.65	0.41	1.18	<0.0001	0.60	0.0358
Biased SSTs- baseline	24.70	0.18	25.93	0.17	35.28	0.36	35.86	0.43	1.23	<0.0001	0.58	0.05
No city	24.77	0.18	24.66	0.09	35.43	0.34	35.71	0.47	-0.11	0.2466	0.28	0.37

Note. The UHI effect is estimated as the urban minus rural difference for observations and each scenario, with bold estimates highlighting significant UHI effect with p-value of 0.05 and lower.

urbanization on the cloud patterns is complex and can vary temporally and spatially. It is important to note that the patchy cloud structures are a result of the relatively short simulation, limiting a point-by-point comparison between these scenarios. However, extending the model integration over a longer duration is expected to reveal more robust and discernible differences. For instance, the cloud frequency climatology by Wilson and Jetz (2016) unambiguously demonstrates that urbanization-related clouds are more frequent than clouds in the surrounding rural areas. This cloud climatology, developed at a 1 km grid size, further reveals intraurban variability in cloud frequency, dependent on urbanization intensity and urban green infrastructures, as observed in the less cloudy areas over the vegetated Addicks and Barker flood control reservoirs in the west of Houston (Figure 1c).

The impact of urbanization in the clouds is more apparent by averaging their properties in space. Figure 8 presents the spatially averaged diurnal-pressure cloud mixing ratio for both the Baseline and the No City scenarios, only considering urban grid points. In general, inland shallow cumulus clouds begin forming early during the daytime, growing deeper and more abundant around 15 LT. The Baseline simulation shows that these clouds are more abundant in the urban areas than in the rural areas, while Baseline minus No City differences further confirm that over built-up land cover these shallow cumuli are more abundant, grow deeper and last longer than over vegetation. Although smaller differences are observed when comparing clouds between the Baseline and No City scenarios in rural areas (not shown), some cloud mixing ratio differences are simulated, likely due to the advection of UHI effects downstream into rural regions (as shown for temperature in Figure 6).

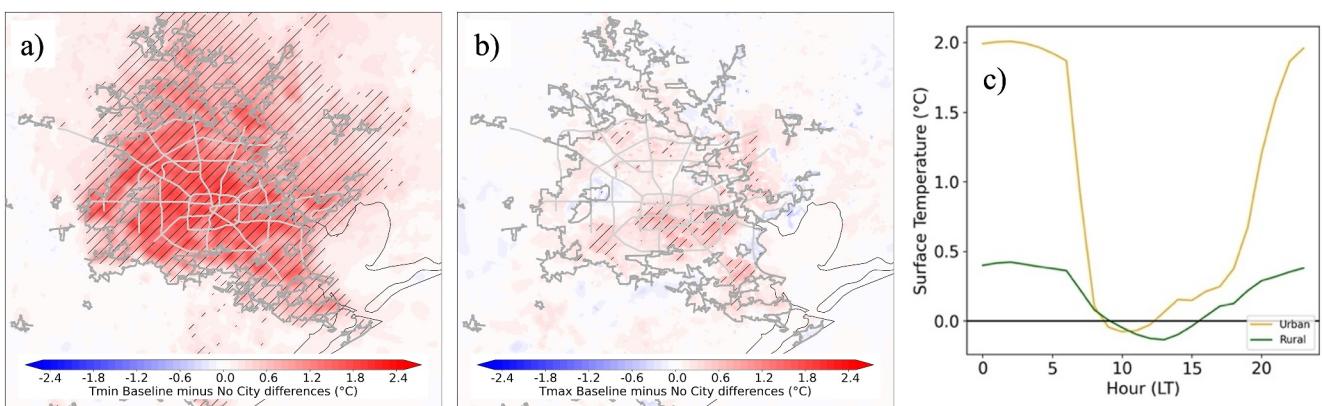


Figure 6. Mean Baseline minus No City differences for (a) T_{min} and (b) T_{max} . Hatched areas in panels (a) and (b) indicate that differences are significant with a 95% confidence level. Dark gray contours indicate urbanization boundaries as of 2010 (Houston-Galveston Area Council, H-GAC; <https://www.h-gac.com/Home>) and light gray show location of major intraurban highways. (c) Spatially averaged diurnal surface temperature for Baseline minus No City differences composed by urban and rural areas.

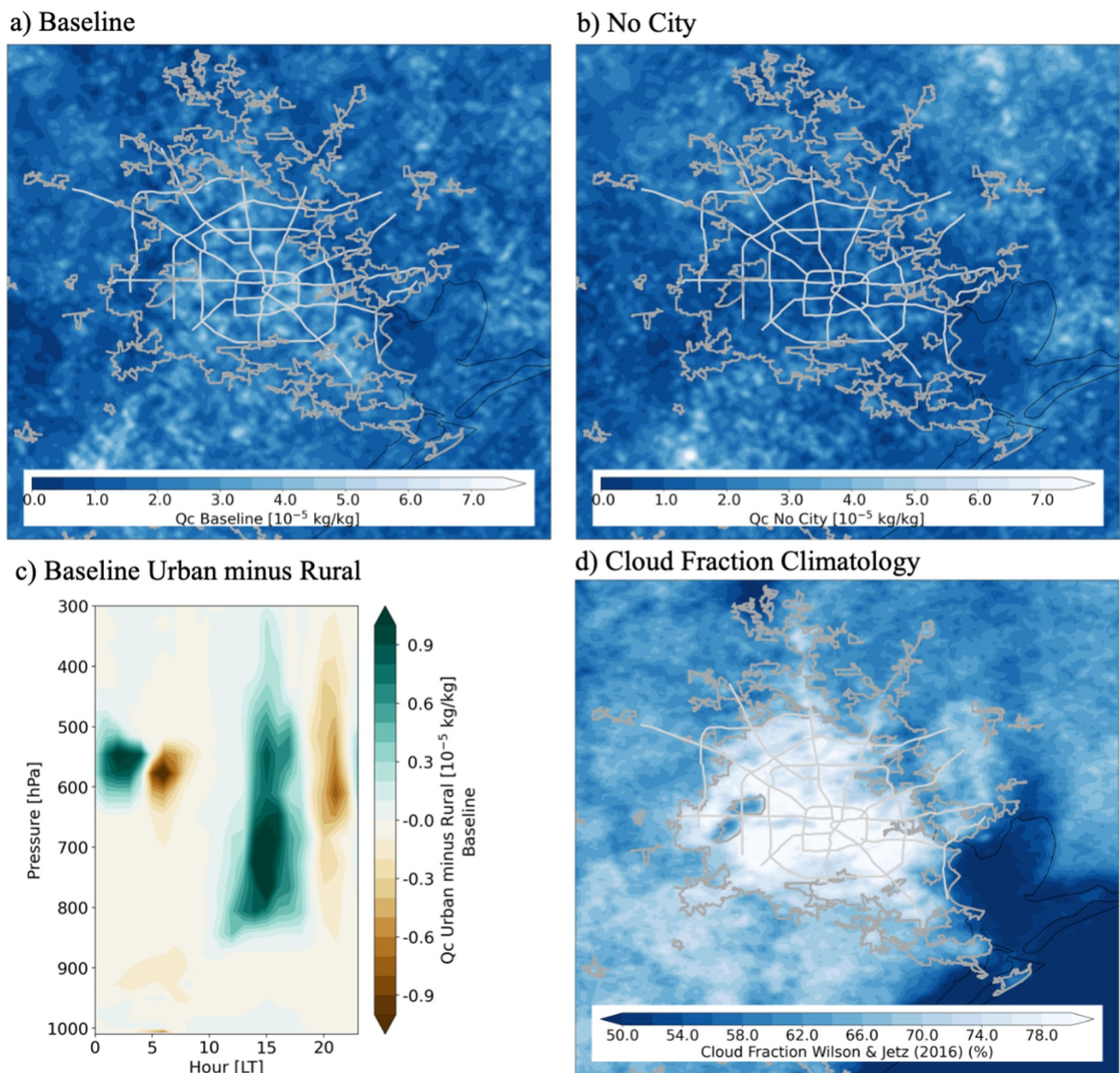


Figure 7. Mean vertical maximum cloud mixing ratio for (a) Baseline and (b) No City scenarios, and (c) Baseline diurnal-pressure urban minus rural composites. (d) Cloud fraction climatology based on 15 years of twice-daily Moderate Resolution Imaging Spectroradiometer (MODIS) satellite images (source Wilson & Jetz, 2016). Dark gray contours indicate urbanization boundaries as of 2010 (Houston-Galveston Area Council, H-GAC; <https://www.h-gac.com/Home>) and light gray show location of major intraurban highways.

Figure 9 shows that the cloud base is significantly higher and thicker (Figure 8) in the urban mixing layer dome. Compared to the rural areas, an increase in cloud base height in the urban area is expected in environments with lower relative humidity (Williams et al., 2015) or higher Bowen ratio (Chiu et al., 2022). Increased Lifting Condensation Level (LCL; as revealed by the increased cloud base height) have been reported over other large urban areas (Han et al., 2022; Shem & Shepherd, 2009). It is possible that the increase in LCL also favors the development of convection, which potentially enhance convective precipitation, as shown in our simulated cloud fields (Figures 7 and 8) and precipitation results (Figure S3 in Supporting Information S1). Additionally, Figure 9 shows a deeper mixed layer over the urban area which is favored by both urban enhanced sensible heat fluxes (Figure 5; Banks et al., 2015; Rahman et al., 2024) and increases in surface friction and urban aerodynamic roughness due to deceleration of the predominant south-southeasterly low-level wind over the urban area (Figures 3d and 10; Rahman et al., 2024).

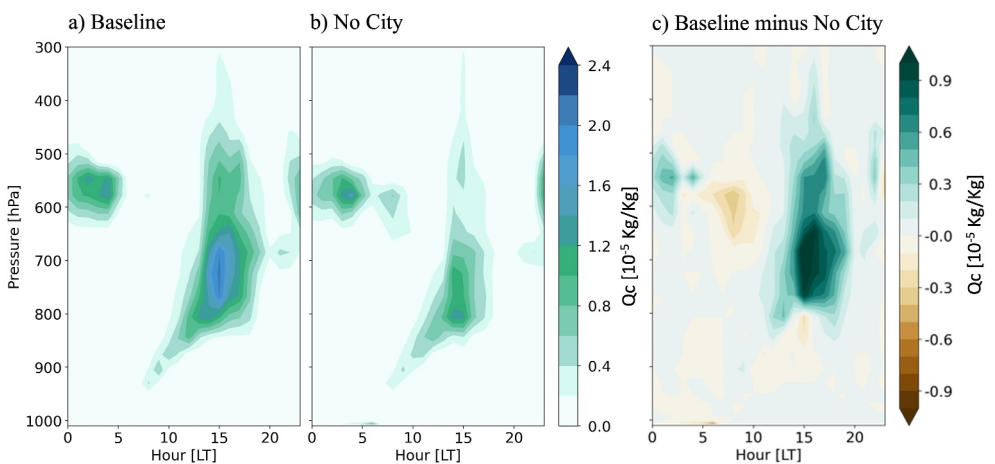


Figure 8. Diurnal-pressure mean urban cloud mixing ratio for (a) Baseline, (b) No City and (c) Baseline minus No City scenarios differences. Urban grid points selected according to MODIS/WUDAPTv2 land use/land cover types.

The diurnal differences of the PBL height shown in Figure 9 reveal that part of the afternoon changes is sensitive to clouds. Notably, the urban PBL diurnal differences increase linearly after sunrise, but are damped around ~ 15 LT, which coincide with the time of maximum shallow cumulus attributed to urbanization (Figure 8c). This potential role of clouds in the PBL evolution is further substantiated when comparing the diurnal differences of the PBL height Baseline minus Clear Sky simulations, which help us partly isolate the role of the sea breeze front. Figure S4 in Supporting Information S1 show that the role clouds in the PBL height is relatively larger compared to those differences based on the Bias SST and No City scenarios; albeit the Baseline minus Biased SST PBL height differences show that warmer SSTs in the Baseline simulation are also related to a dip in the PBL height around 15 UTC (Figure S4 in Supporting Information S1). Hence, urban related shallow cumulus help control the transient surface cooling effect and sensible heat flux reduction (Figure 5), temporarily suppressing the vertical mixing. Section 3.4 further disentangles the role of urban and coastal processes on shallow cumulus clouds.

To better understand the factors driving enhanced clouds over the urban dome, we examined the diurnal-height urbanization impacts for various dynamical and thermodynamical parameters, using composites of the Baseline minus No City scenarios (Figure 11). Synchronous with enhanced afternoon uplift, the urban dome extends up to ~ 2 km with a dipole of warmer and drier airmass over the city and cooler and moister air mass in the upper-mixing layer. A significant feature in Figure 11 is that the mixed layer air entering the afternoon shallow cumulus clouds

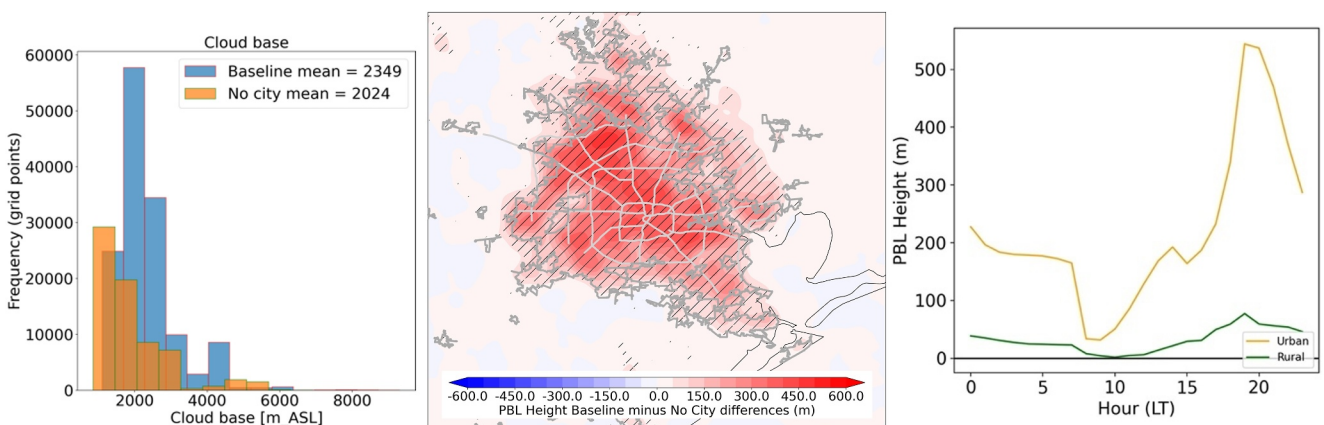


Figure 9. (Left panel) Cloud base distribution for the Baseline and No City scenarios over the urbanized area. Student's t -test and Kolmogorov-Smirnov test indicate that means and distributions are significantly different with 99% confidence level. (Middle panel) Baseline minus No City planetary boundary layer (PBL) height differences with hatched areas indicating that differences are significant with a 95% confidence level; Dark gray contours indicate urbanization boundaries as of 2010 (Houston-Galveston Area Council, H-GAC; <https://www.h-gac.com/Home>) and light gray show location of major intraurban highways. (Right panel) Baseline minus No City PBL height differences averaged over urban and rural areas.

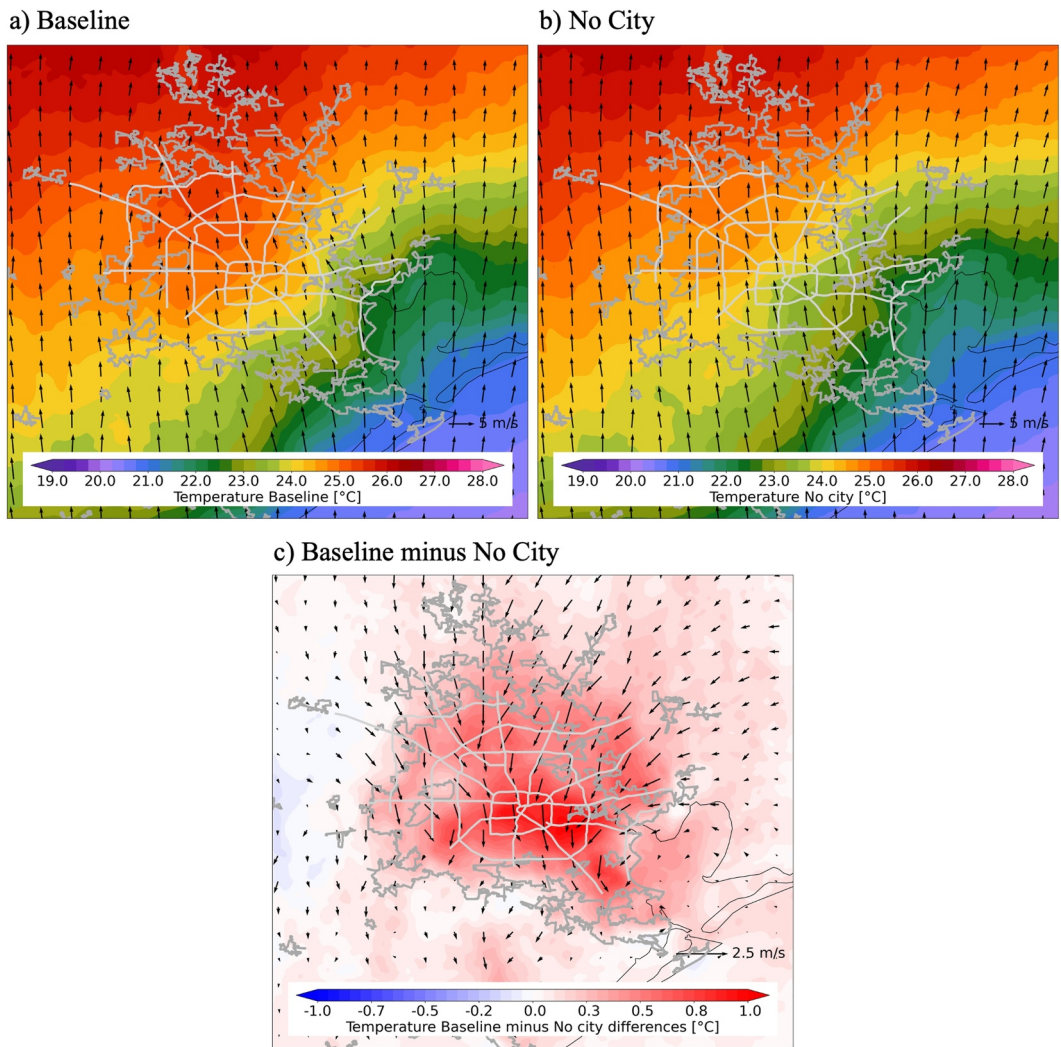


Figure 10. Mean 500 m (above MSL) temperature and wind vectors for (a) Baseline, (b) No City, and (c) Baseline minus No City differences averaged between noon and 18 LT. Dark gray contours indicate urbanization boundaries as of 2010 (Houston-Galveston Area Council, H-GAC; <https://www.h-gac.com/Home>) and light gray show location of major intraurban highways.). Wind vectors are plotted only every 6 grid points to avoid cluttering.

is related to enhanced Moist Static Energy (MSE), suggesting that the clouds convective updrafts (Figure 11b) are dominated by the warmer temperatures (Figure 11a) and increased sensible heat fluxes near the surface, as well as enhanced water vapor in the upper-mixed layer (Figure 11c). Dynamically, the enhanced water vapor air masses are sustained by the increases in both horizontal moisture flux convergence at low-levels and upward moisture flux convergence in the upper-mixed layer. Additionally, an urban-induced circulation cell with northerly low-level and south-southwesterly upper-mixed layer circulation disturbance (and enhanced moisture flux divergence) is revealed. This circulation pattern in the urban dome resembles the self-contained UHI circulation described by Fan et al. (2017). Moreover, Figure 10 highlights the horizontal extent of the low-level branch of this circulation, impacting beyond the urban area and well downstream of the city. Upstream and toward the coast, however, urbanization circulation sensitivity overwhelms any potential influence of the city on the sea breeze.

It is possible that shallow cumuli and enhanced precipitation (not shown) moisten the cloud and subcloud layers, further favoring more cloud development. Figure 12 displays a bulk mixing line analysis with the thermodynamical structure of conserved variables (potential temperature and water vapor mixing ratio) in the subcloud and surface layers. The enhanced frequency in entrainment and downdrafts zones in the Baseline relative to the No City simulation further suggest more active cloud dynamics. Notably, when compared to the No City simulation,

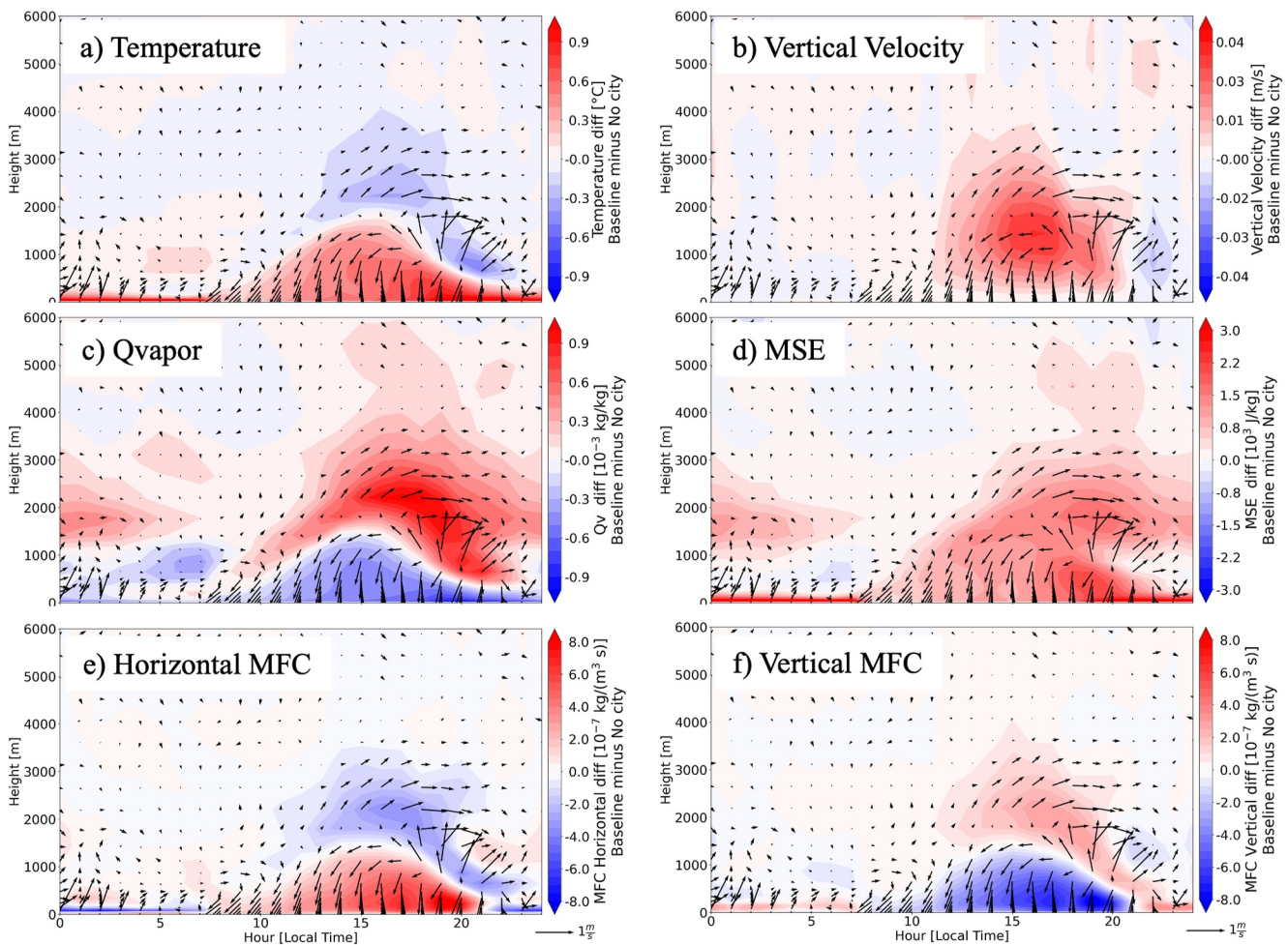


Figure 11. Diurnal-height Baseline minus No City scenario differences spatially averaged over the urban areas for (a) air temperature, (b) vertical wind component, (c) water vapor mixing ratio, (d) moist static energy (MSE), (e), horizontal moisture flux convergence, and (f) vertical moisture flux convergence. Vectors in each panel correspond to the horizontal wind, with the north direction pointing upwards. In the vertical, wind vectors are plotted only every 6 grid points to avoid cluttering. $MSE = C_p \cdot T + g \cdot z + L_v \cdot q$, where C_p is the specific heat at constant pressure, T is the air temperature, g is the gravitational constant, z is the geopotential height above MSL, L_v is the latent heat of vapourization, and q is the specific humidity.

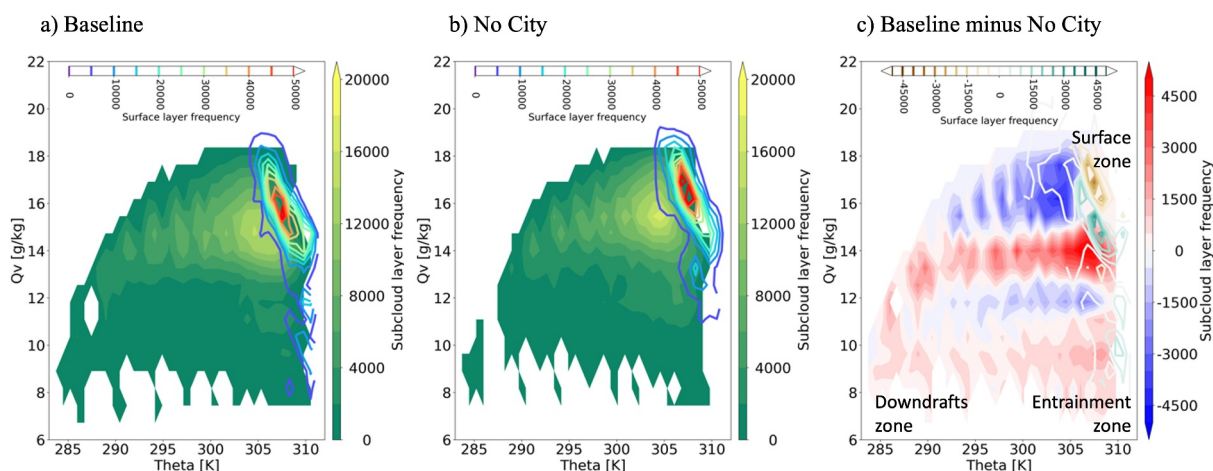


Figure 12. Mixing line potential temperature and water vapor mixing ratio frequency distribution analyses for (shaded contours) subcloud and (contour) surface layers over the urban area for (a) Baseline, (b) No City, and (c) Baseline minus No City. Only urban grid points in the 12 to 16 LT period were considered.

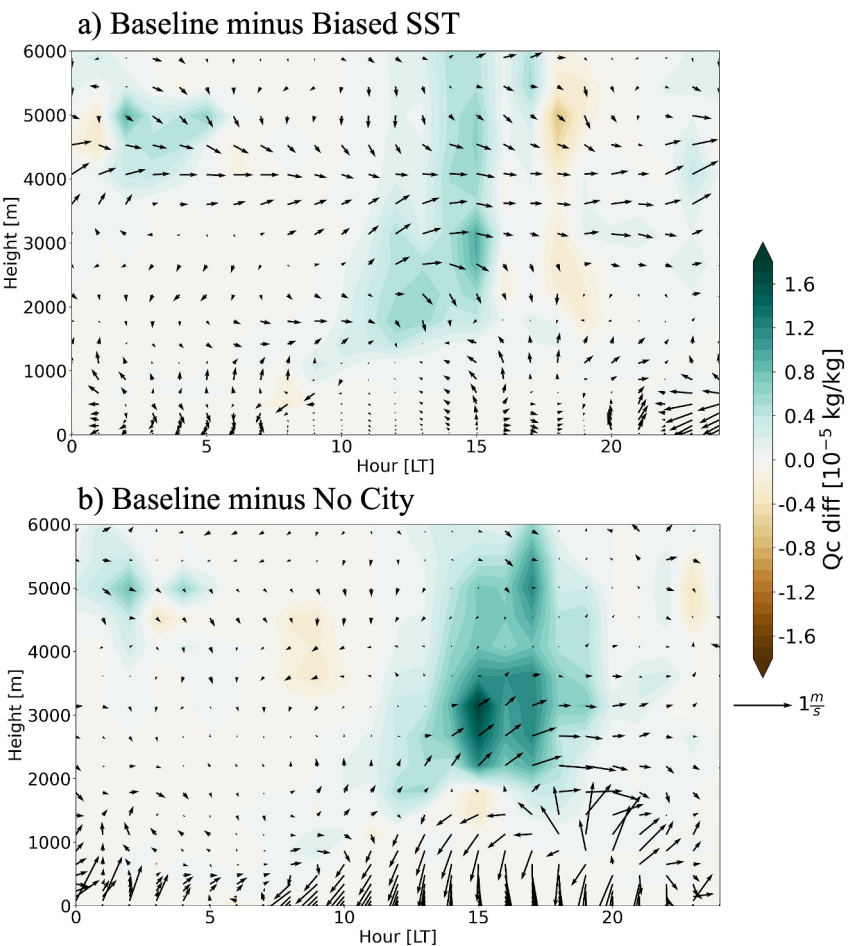


Figure 13. Diurnal-height Cloud mixing ratio and wind vector differences spatially averaged over the urban areas for (a) Baseline minus Biased Sea Surface Temperature and (b) Baseline minus No City. Vectors in each panel correspond to the horizontal wind, with the north direction pointing upwards).

the Baseline simulation shows that surface fluxes predominantly provide a warmer and dryer mixing lines, with enhanced downdrafts moistening and cooling the subcloud layer. The enhanced cloud downdrafts help explain the layer of relatively cool air above the UHI dome shown earlier (Figure 11a). Furthermore, the Baseline simulation also shows more air masses with warming and drying turbulent entrainment from the free atmosphere into the subcloud layer. Thermodynamically, the enhanced MSE in the subcloud layer (Figure 11d) is then predominantly maintained by enhanced enthalpy from the surface zone, and partly enhanced by evaporation of the downdrafts and turbulent entrainment. A MSE budget can reveal the proportion of MSE fluxes from each zone, but we refrained to further diagnose the zone contribution fraction because by construction, the non-local closure PBL scheme used in our modeling setup limits a detailed characterization of the mixing lines within the mixed and subcloud layers.

3.4. Sea-Breeze and Urban Induced Circulations

To test the sensitivity of the urban clouds against regional sources of moisture and mesoscale circulations related to the land-sea contrast, we compared the Baseline with the Biased SST simulations. Figure 13 shows that the warm SSTs adjustment in the Baseline simulation favors more shallow cumulus clouds. The effect of urbanization, however, is still dominant when compared to the warm SSTs adjustment. Notwithstanding is that the warm SSTs adjustment also increases clouds over the rural areas (not shown). By construction, the warmer SSTs develop a warmer low-level atmosphere, with increased latent heat fluxes and water vapor, that in turn, are advected by the predominant southerly and southeasterly flow (Figures 3 and 10). Figure 14 shows evidence of warming and moistening over the city, with some striking asymmetries in relation to the changes in local

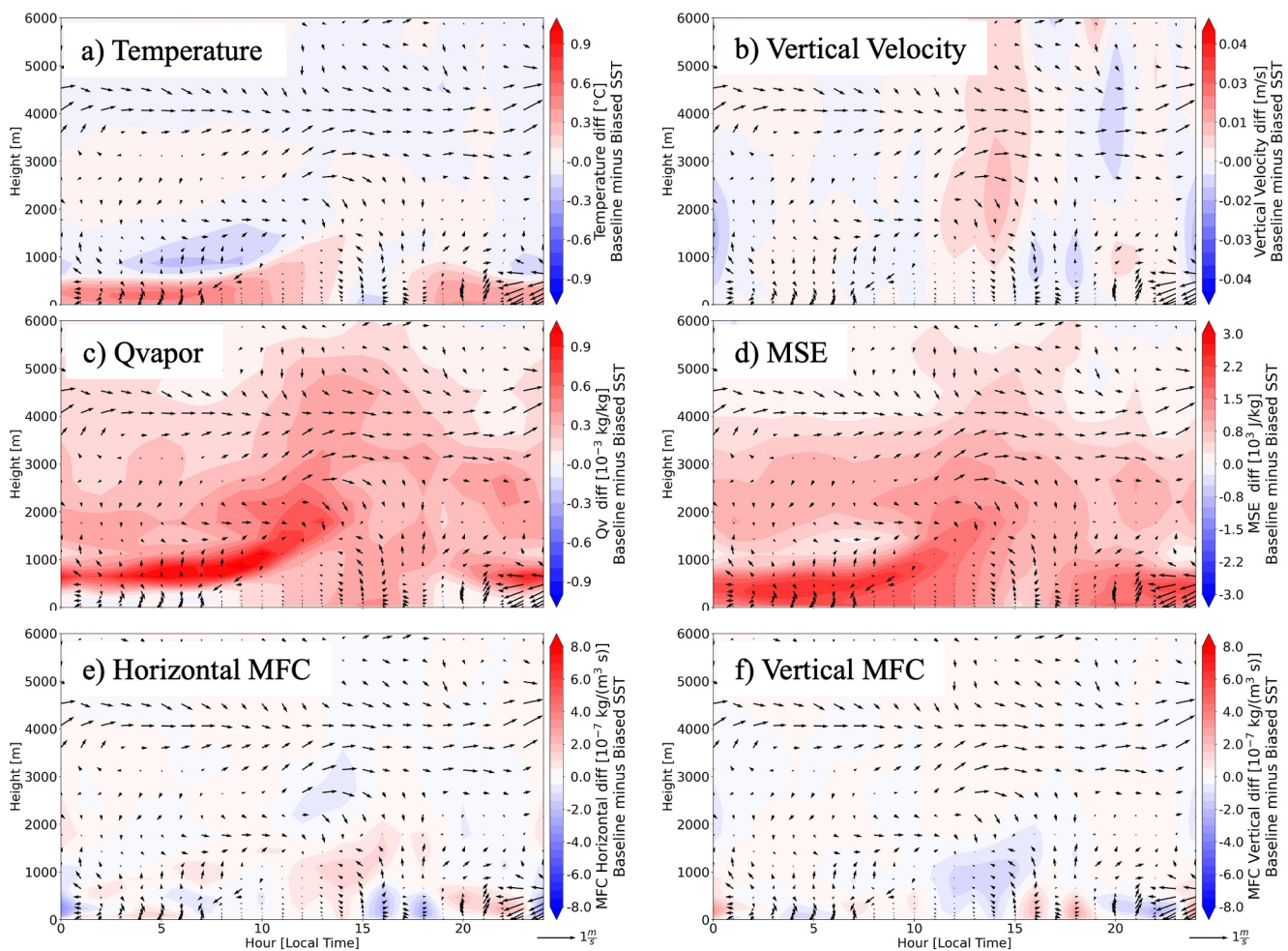


Figure 14. Same as Figure 11 but for Baseline minus Biased Sea Surface Temperature scenario differences. Vectors in each panel correspond to the horizontal wind, with the north direction pointing upwards. Wind vectors are plotted only every 6 grid point to avoid cluttering.

circulation and the clouds themselves. The increased water vapor and temperature are related to the more intense MSE signal, which favors a thermodynamical pathway for the enhancement of clouds due to a more unstable lower troposphere, with an enhanced, but weaker relative to the Baseline minus No City, horizontal MFC support. Notably, the urban area shows a low-level cooling and moistening signal concurrent with the enhanced clouds, further displaying the role of the urban clouds and subcloud layer processes in the daytime UHI effect.

To better display the impact of the No City and Biased SSTs in the mesoscale circulations, Figures 15 and 16 show 6-hr averaged diurnal time slices for both interpolated fields at 500 m height and latitude-height slices across the city (Figure 1c). The Baseline minus No City differences show that the urban circulation dome is emphasized as the warm blob collocated with the northerly wind differences. Earlier results showed that this urban circulation dome is favored by the enhanced sensible heat flux, increasing the urban-rural thermal gradient and vertical mixing over the city, and the dynamic frictional drag due to urban enhanced friction and building blocking. Of note is that urbanization imposes anticyclonic and cyclonic differences to the west and east of the city core, respectively, with a horizontal scale as large as the urbanization scale and extending vertically as high as 3,500 m above MSL (Figure 15; Fan et al., 2017).

Isolating the role of the sea-breeze and urban induced circulations on the enhanced afternoon clouds is challenging. Afternoon (12–18 LT) composites in Figures 15 and 16 show that the urban circulation dome seems to dominate the Baseline minus No City circulation difference, overwhelming impacts on the land- and sea-breeze circulation that have been reported in the literature (Fan et al., 2020; Rahman et al., 2024; Ryu et al., 2016; Shen et al., 2018; Wang et al., 2023). This aspect holds for hourly mean composites or individual sea breeze fronts (not shown). Above the

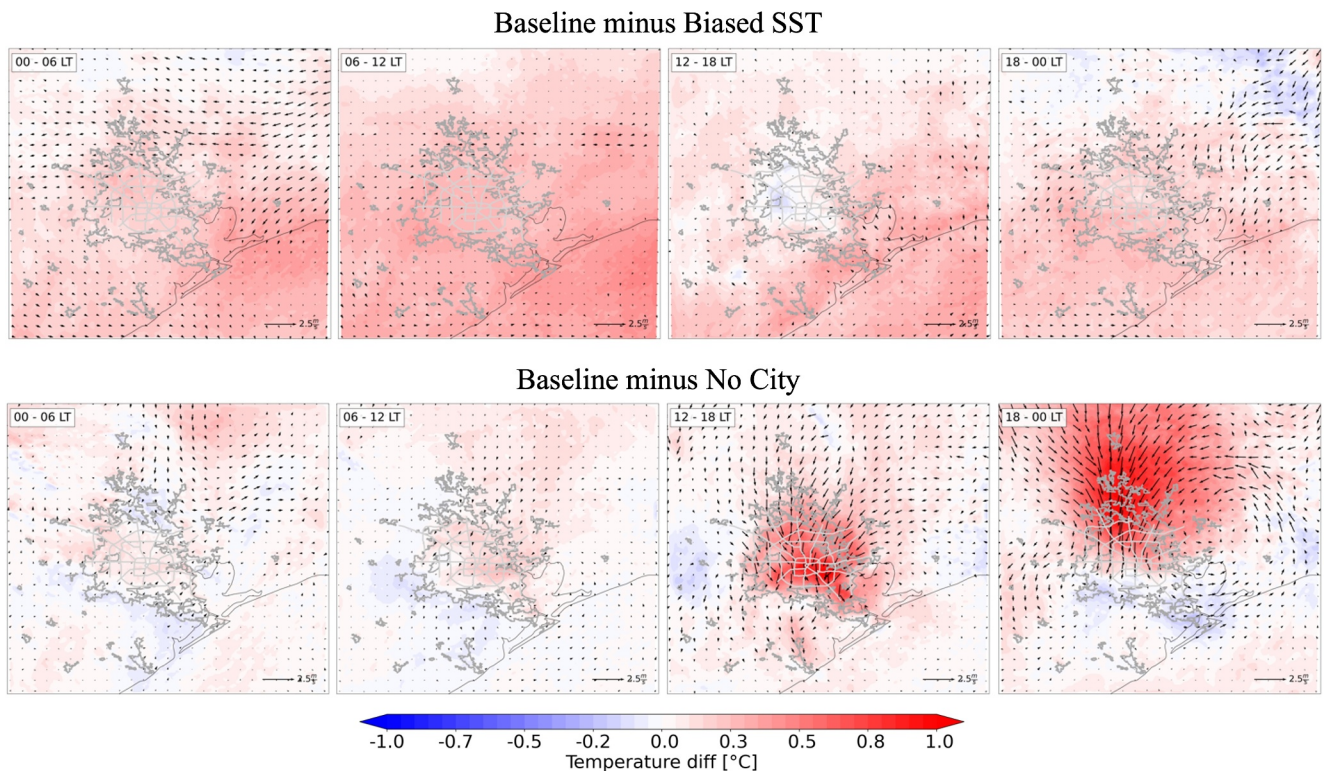


Figure 15. 500 m (above MSL) height air temperature (contours) and horizontal circulation (vectors) for (top panels) Baseline minus Biased SSTs and (bottom panels) Baseline minus No City differences, diurnally averaged over 6-hr time slices (upper left corner in each panel; LT). Wind vectors are plotted every 10 grid point to avoid cluttering. Dark gray contours indicate urbanization boundaries as of 2010 (Houston-Galveston Area Council, H-GAC; <https://www.h-gac.com/Home>) and light gray show location of major intraurban highways.

urban heat dome, Figure 16 also reveal a coherent southerly, cooler urban induced flow, related to the return branch of the rural-urban cell. Earlier (Figure 11), we showed that above the urban heat dome this urban induced cooling feature could be partly related to enhanced cloud pathways, which favors enhanced downdrafts moistening and cooling the cloud and subcloud layers. During the evening (18-00 LT), Figure 16 also shows elevated cooling feature located south of the city and over the rural area, with distinct low-level urban-related northerly differences and elevated, southerly flow favoring advection of cooler and more humid air masses (shown in Figure 11c) from the rural and maritime environment above the heat dome and into the urban area.

The impact of warmer SSTs in the Baseline simulation shows an enhancement of the evening-to-morning land-breeze and a weaker sea-breeze (Figure 15), which agrees with previous SST sensitivity studies (Chen et al., 2011; Ryu et al., 2016). Characterizing the timing and intensity of the sea breeze in the Houston-Galveston area is complicated by the costal shapes and SST differences with a relatively warmer Galveston Bay as compared to the Gulf of Mexico (Salas-Monreal et al., 2018). However, Figure 16 shows that the weaker sea breeze cell favors the weaker moisture transport near the surface and augments the southerly southeasterly flow in the return branch of the cell, which help describe the moist difference over the urban area (Figure 14c). Additionally, the enhanced offshore sensible and latent heat fluxes in the Baseline simulation help develop a deeper and moister marine boundary layer (not shown), further enhancing the transport of water vapor by the background wind and in the return branch of the sea-breeze.

3.5. Heat Index Sensitivity

Here, we examine the role of urbanization, clouds, and SST uncertainties in the HI. Figure 2 indicated that the model has some limitations in simulating the amplitude of the diurnal cycle of the HI over both rural and urban areas, overemphasizing the HI during the nighttime and underemphasizing the HI during the daytime. Although these diurnal biases can be traced to a low performance in simulating relative humidity, more work is needed to assess the model limitations and sources of uncertainty in estimating the HI. By contrasting the model simulation

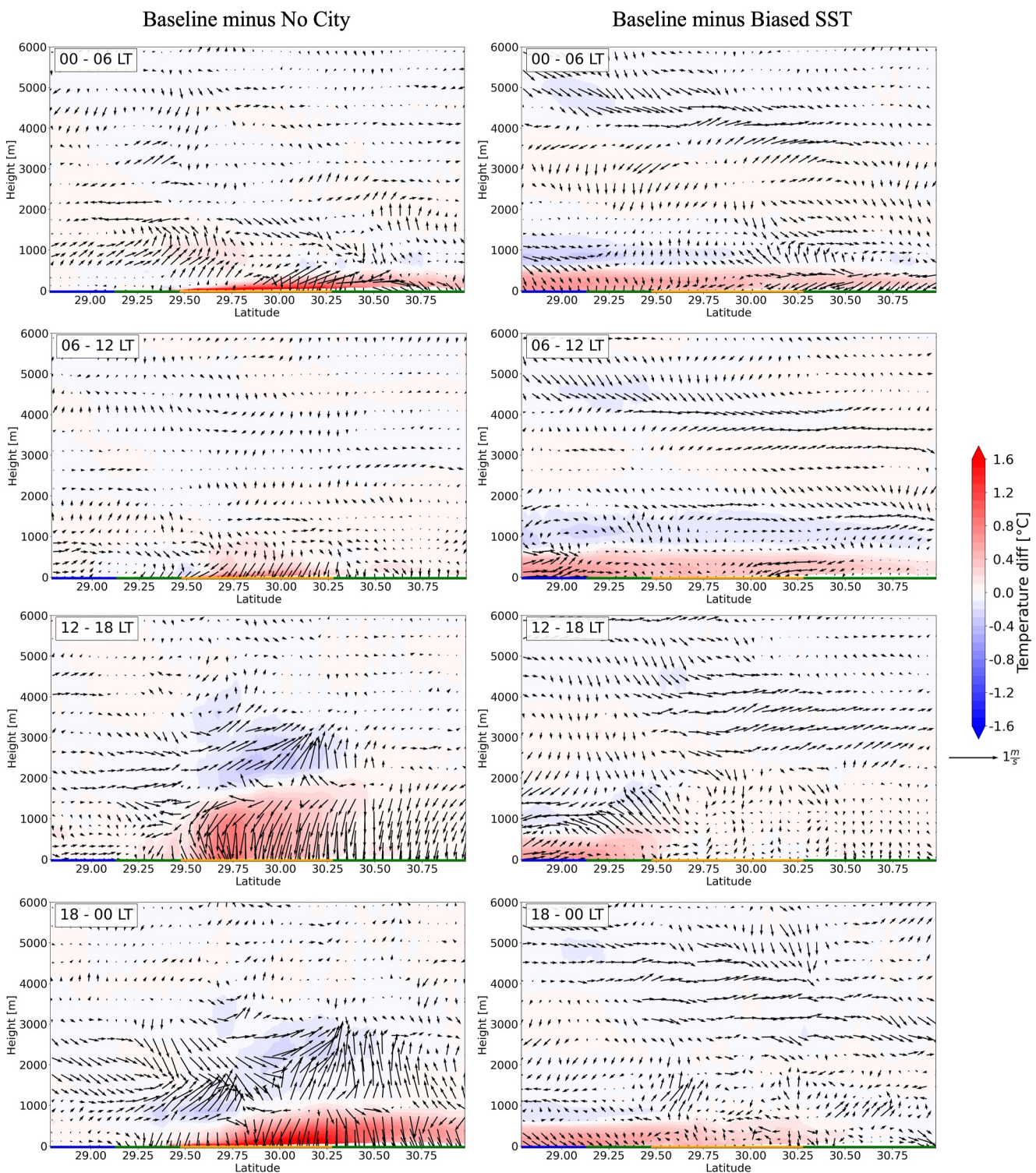


Figure 16. Diurnal evolution (top to bottom) of latitude-height temperature and wind vectors for Baseline minus No City and Baseline minus Bias Sea Surface Temperature analyses along transect displayed in Figure 1, with colored lines at the bottom of the panels indicating the location of water (blue line), rural (green lines) and urban areas (orange line). Vectors in each panel correspond to the horizontal wind, with the north direction pointing upwards.

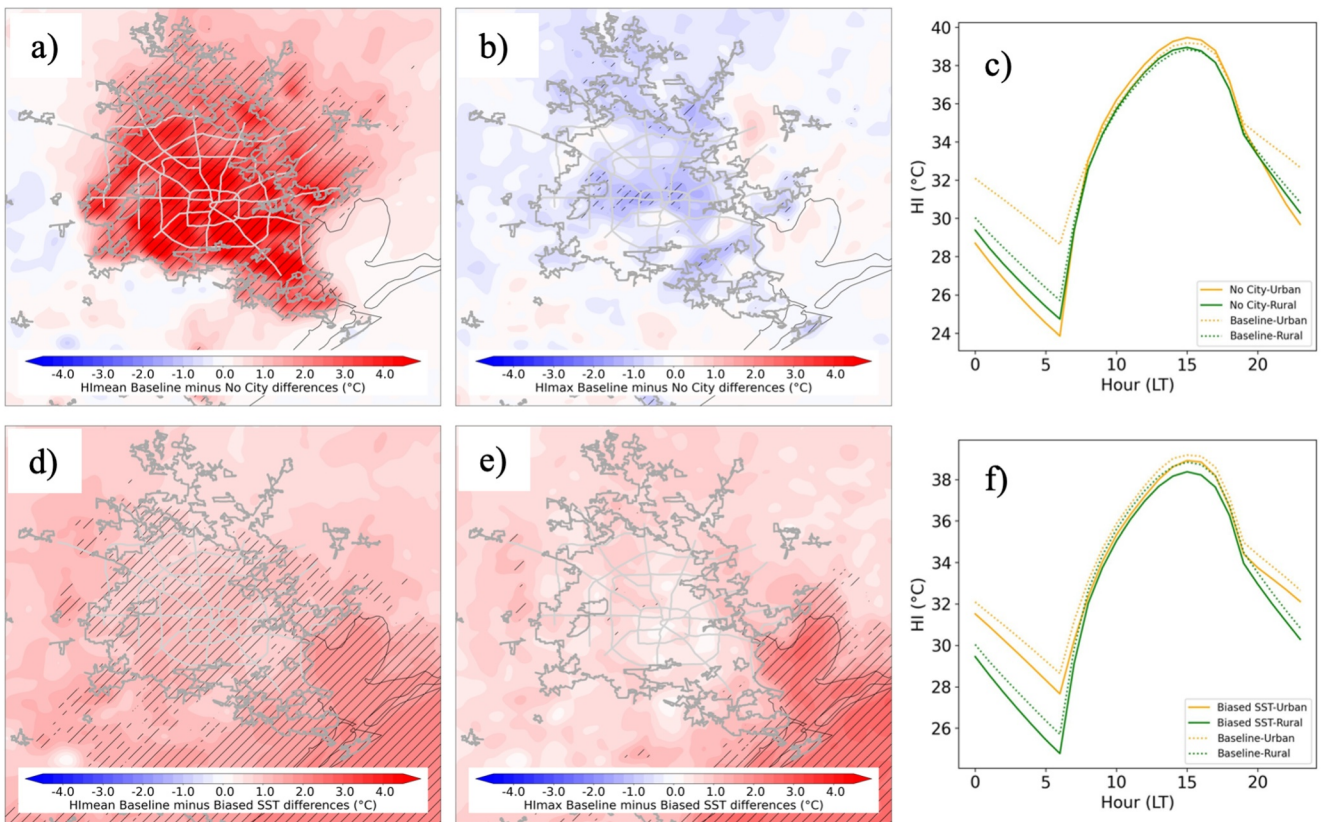


Figure 17. Diurnal mean and maximum Heat Index (HI) differences for Baseline minus No City (a, b, respectively) and Baseline minus Biased Sea Surface Temperature (d and e, respectively). Hatched areas indicate that differences are significant with a 95% confidence level; Dark gray contours indicate urbanization boundaries as of 2010 (Houston-Galveston Area Council, H-GAC; <https://www.h-gac.com/Home>) and light gray show location of major intraurban highways. HI diurnal variability composited by rural and urban areas is also added for (c) Baseline and No City and (f) Baseline and Biased SST.

scenarios, however, we can partly cancel these biases (i.e., linearizing the potential effect of internal feedbacks) and retain the signal related to urbanization, clouds and SST in the diurnal evolution of the HI.

Figure 17 shows the sensitivity of the HI to urbanization and SST adjustments. On the mean, the UHI has a significant influence in increasing the HI, mostly during the nighttime and early morning. During high HI times (around 15 LT), however, urbanization is related to weaker HI compared to the rural areas, due to the competing impacts of air temperature and relative humidity on the HI. Over the city, the weaker high HI is partly due to the urban dry island effect (Figure 5c), and partly due to enhanced clouds and its surface cooling effect (Figure 8), limiting high temperatures in the city (Figure 6). The sensitivity of the HI to moisture is also shown when contrasting Baseline with the Biased SST simulation. Figure 17 also shows that the warmer SSTs ($\sim 1^{\circ}\text{C}$) impact the mean HI with a more intense effect near the coast and over the urbanized areas. During high HI, the HI impact of the warmer SSTs over the urban area is less apparent, likely due to the cloud surface cooling effect balancing the warmer and moist sea breeze (Figure 14).

4. Discussion and Conclusion

To better understand the effect of urbanization in meteorology over the Houston-Galveston area, this study developed 900 m grid size simulations between 1 and 16 August 2020 using a cloud- and urban-resolving atmospheric model that includes a Building Energy Model coupled with BEP. The study investigates the intricate interplay of clouds in local weather, considering various influencing factors. Several model realizations were developed to isolate the role of the urban environment and the clouds and to address SST uncertainties in the complex Galveston Bay and Gulf of Mexico coast and its effect in the land-sea circulations known to affect the urban climate (Chen et al., 2011; Fan et al., 2020; Ngan et al., 2013). By excluding local anthropogenic aerosols and their effects, this research provides deeper insights into the relationship between the city and shallow cumulus

clouds. These insights contribute to our understanding of the processes modulating excessive heat indicators over urban environments.

Results showed that Houston-Galveston urbanization favors more shallow cumulus clouds. Our modeling and satellite results show an apparent cloud enhancement due to urbanization, in agreement with the findings based on satellite data by Vo et al. (2023); of note is that the simulation period for this study coincides with the time of the year when the urbanization cloud patterns are the largest for Gulf Coast coastal cities (Vo et al., 2023). These results agree with the hypothesis that even over urban areas with relatively drier environments, the surface-driven turbulence can sustain longer-lasting clouds compared to the surrounding rural areas (Loughner et al., 2011; Theeuwes et al., 2019). Despite the model uncertainties and biases, and without considering the role of aerosols, relevant for cloud and precipitation invigoration (Fan et al., 2020) in urban environments, our results help understand the mechanistic processes involved in the urban cloud enhancement.

Particularly, our simulations confirm the control of the UHI in the clouds by enhanced vertical mixing due to aerodynamical drag and an enhanced sensible heat, as compared to the surrounding rural areas. In addition, our results also offer a deeper insight on the dynamic and thermodynamic interplay in the cloud enhancement. The city sustains more clouds, with higher cloud heights and deeper shallow cumulus owing to enhanced MSE, partly due to enhanced enthalpy by the surface sensible heat and partly due to the enhanced latent heating favored by a stronger low-level horizontal moisture flux convergence (Chiu et al., 2022; Fan et al., 2017; Loughner et al., 2011; Theeuwes et al., 2021). We showed that more clouds, in turn, are related to a cooler surface temperature maximum, when compared to the No City environment and the surrounding rural areas. This cooling can further reduce the afternoon urban-rural heating contrasts and suppress vertical mixing. However, our mixing line analysis also shows that part of this cooling can also be attributed to evaporative cooling by downdrafts. Notwithstanding, enhanced MSE is predominantly maintained by the surface heat fluxes, with a minor role from the warm air entrainment fluxes. All these mechanisms also help understand the precipitation enhancement associated with urbanization (Figure S3 in Supporting Information S1; Chiu et al., 2022; Fan et al., 2020; Lorenz et al., 2019; Ryu et al., 2016; Statkewicz et al., 2021, Wang et al., 2023; Zhu et al., 2016) and aerosol-cloud interaction and air pollution impacts (Caicedo et al., 2019; Fan et al., 2020; Loughner et al., 2011; Seigel, 2014; Zhong et al., 2015, 2017), which are ongoing observational and modeling research foci (Jensen et al., 2022).

Our results suggest that the enhanced roughness and building barrier effects, sensible heat, and vertical mixing related to urbanization act as an obstacle to the prevailing flow, favoring urban circulation dome patterns with a horizontal scale of influence as large as the urban area. Previous studies have suggested that the UHI circulation can strengthen the sea breeze circulation, which favors moisture flux convergence and cooler airflow the urban environment enhanced (Fan et al., 2020; Ryu et al., 2016; Shen et al., 2018; Zhong et al., 2017). However, vertical mixing acts as obstacles to prevailing flows, with a scale of influence that appears to overwhelm the thermal-driven bay- and sea-breezes influencing the city. It is possible that deceleration from the urban roughness and building barrier effects becomes less prominent, and the urban land effect on the sea breeze circulation can become more evident, during weaker or different south-southwesterly background flow regimes (Chen et al., 2011; Ngan et al., 2013; Wang et al., 2022).

Urbanization increases the mean HI, but the maximum HI is less intense in the urban area of the Baseline simulation, due to the cloud enhancement pathway that acts as a cooling mechanism. Additionally, the model sensitivities to SSTs revealed that the coastal environment can modulate the UHI intensity, with warmer SSTs producing cooler urban surface temperature highs due to enhancement of the established shallow cumulus cloud pathway, due to the warmer and moister sea breeze. Near the coast, the effect of the warmer and more humid environment (due to the warmer SSTs) advected by the sea-breeze appears to have a net intensification of the urban HI, but the maximum HI does not show significant sensitivity, likely due to the competing factors between the surface temperature and relative humidity. These results offer new insights and complement other studies focusing on urbanization and related modulation of the sea breeze as driving mechanisms of the urban heat stress and pollution transport problems in cities near large surface water bodies (Caicedo et al., 2019; Shen et al., 2018; Wang et al., 2023).

Through comprehensive model evaluation using 242 surface station sites, an upper-air wind profiler and a cloud climatology, our analyses reveal that the model simulations perform adequately, but common and well-documented biases remained. For instance, the model overestimates the strength of the sea breeze, consistent

with the urban warm surface temperature bias (Figure 2) and a more intense nighttime temperature gradient, maintaining the onshore sea-breeze flow much longer. Likewise, the warm nighttime bias could be partly related to the overemphasized low-level southerly winds by enhancing the temperature advection from the offshore waters into land and the urban areas. Consequently, all results and conclusions relying on advection of environmental parameters, into or downstream the city need to be assessed with caution. For example, the downstream extend of the UHI impact to the north and northeast of the city may be overemphasized due to the strong wind bias. Over rural areas, the warm and dry bias could be related to over advection of the UHI and urban dry island effects (Qian et al., 2022; Figure 4). This agrees with the bias differences between the urbanized (Baseline) and the No City simulations, showing that the city modulates part of the surface temperature errors, even over the rural areas (UHI advection and UHI dome and related circulations).

It has been suggested that the UHI is more pronounced during the nighttime (Oke, 1982), but recent studies have found asymmetries in the time of the maximum diurnal UHI effect, arguing that vegetation type, urban and rural activities (Peng et al., 2012), or clouds (Vo et al., 2023) can affect the time of its maximum. Surface station estimates in the study area and period suggest that the afternoon UHI was more intense than the morning UHI, whereas the model suggested the opposite. This UHI intensity disagreement between model and surface stations is common (Hu et al., 2019; Qian et al., 2022; Venter et al., 2021). However, estimating the magnitude of the UHI based on surface station observations is a challenging task, including potential observational uncertainty issues related to limitations of urban stations in following footprint standards (WMO, 2008). Moreover, the magnitude of the UHI is more pronounced farther from the coast, but also varies according to the location of the rural stations relative to the predominant low-level flow, due to the outlined advection of heat downstream from the city.

Our results show the typical ground heat flux driving the nighttime UHI, but other meteorological factors became apparent when considering the interaction with mesoscale circulations and clouds. During the afternoon, we speculate that the smaller simulated diurnal UHI can include possibly the over estimation of the urban clouds, limiting temperature highs in the afternoon, asymmetries in the biases between urban and rural sites, among other model deficiencies. During the nighttime, urbanization enhanced clouds can slow nighttime longwave radiation cooling.

Modeling work aiming to assess the impact of heat adaptation and mitigation strategies need to assess the tradeoffs in the UHI circulations and clouds pathways relationships. Most mesoscale urban heat mitigation modeling studies suggest different cooling strategies influencing city scale net cooling effects ranging from ~ 0.1 to a few degrees Celsius, depending on the intensity of the implementation (Krayenhoff et al., 2021), but often assume that model biases and other errors are somehow steady under different model conditions and disregard the effect of model errors on relevant physical process. Hence, the impact of cooling strategies can be overwhelmed by uncertainties in SST fields (i.e., those related to observations and data assimilation uncertainties), or by the accuracy of the simulated clouds and precipitation, which is typically an important source of uncertainty in the model.

Data Availability Statement

Surface Station Data: All the observational data needed to develop this study is readily available online. This research utilized weather observations from NWS, RAWS, TCEQ, CAMS networks and were obtained using the Synoptic Data PBC Mesonet API (free access to the data via <https://mesowest.utah.edu/>); buoy implemented is readily accessible in the NOAA data portal (<https://www.ndbc.noaa.gov/>).

Wind Profiler Data: The Cooperative Agency Profilers data set can be accessed online using NOAA data portal <https://madis-data.ncep.noaa.gov/cap/> (last access, 04/02/2024).

The Model: The Weather and Research Forecasting model (WRF) is freely available and maintained by the UCAR/National Center for Atmospheric Research (https://www2.mmm.ucar.edu/wrf/users/download/get_source.html) with source version control in the Github portal (<https://github.com/wrf-model/WRF/releases>).

Local Climate Zones Data: Urban Land Cover/Land Use data used in this study were obtained and distributed by Demuzere et al. (2022a, 2023) and postprocessing code were made available by Demuzere, Argüeso, et al. (2022). This data set complements the data for individual cities from the World Urban Database and Access Portal (WUDAPT; <https://www.wudapt.org/>).

Sea Surface Temperature (SST) Data: SST used is based on the Advanced Very High Resolution Radiometer on the European MetOp satellites, and the Visible Infrared Imaging Radiometer Suite (VIIRS) on the U.S. SNPP and NOAA JPSS satellites NOAA-SNPP VIIRS and readily available online (https://eastcoast.coastwatch.noaa.gov/cw_data_access.php).

Initial and Boundary Conditions: The Global Tropospheric Analyses and Forecast Grids a (GDAS/FNL; 0.25°) were used as initial and boundary conditions to drive the WRF model and is readily accessible online (<https://rda.ucar.edu/datasets/ds083.3/>; <https://doi.org/10.5065/D65Q4T4Z>).

Acknowledgments

This work was funded by NOAA-Climate Program Office Extreme Heat Risk Initiative Grant NA21OAR4310149. City of Houston—Mayor's Office of Resilience and Sustainability and National Weather Service Forecast Office (Timothy Cady), Houston-Galveston, TX for their support in this study. High-performance computing was partially provided the University of Nevada's Office of Information Technology, Research & Innovation, and the Nevada Governor's Office for Economic Development. We extend our thanks to Drs. Zonato Andrea and Alberto Martilli for their insight in numerical diffusion issues in earlier versions of our model configurations. The authors express gratitude to the anonymous reviewers for their valuable input and insightful comments.

References

- Ancell, B. C., Bogusz, A., Lauridsen, M. J., & Nauert, C. J. (2018). Seeding Chaos: The Dire consequences of numerical noise in NWP perturbation experiments. *Bulletin America Meteorology Social*, 99(3), 615–628. <https://doi.org/10.1175/BAMS-D-17-0129.1>
- Banks, R. F., Tiana-Alsina, J., Rocadenbosch, F., & Baldasano, J. M. (2015). Performance evaluation of the boundary-layer height from Lidar and the weather research and forecasting model at an urban coastal site in the north-east Iberian Peninsula. *Boundary-Layer Meteorology*, 157(2), 265–292. <https://doi.org/10.1007/s10546-015-0056-2>
- Blackadar, A. K. (1957). Boundary layer wind maxima and their significance for the growth of nocturnal inversions. *Bulletin America Meteorology Social*, 38(5), 283–290. <https://doi.org/10.1175/1520-0477-38.5.283>
- Bouali, M., & Ignatov, A. (2014). Adaptive reduction of Striping for improved sea surface temperature imagery from Suomi National Polar-Orbiting Partnership (S-NPP) visible Infrared imaging Radiometer Suite (VIIRS). *Journal of Atmospheric and Oceanic Technology*, 31(1), 150–163. <https://doi.org/10.1175/JTECH-D-13-00035.1>
- Brousse, O., Martilli, A., Foley, M., Mills, G., & Bechtel, B. (2016). WUDAPT, an efficient land use producing data tool for mesoscale models? Integration of urban LCZ in WRF over Madrid. *Urban Climate*, 17, 116–134. <https://doi.org/10.1016/j.uclim.2016.04.001>
- Cady, T. J., Rahn, D. A., Brunsell, N. A., & Lyles, W. (2020). Conversion of abandoned property to green space as a strategy to mitigate the UHI investigated with numerical simulations. *Journal of Applied Meteorology and Climatology*, 59(11), 1827–1843. <https://doi.org/10.1175/JAMC-D-20-0093.1>
- Caicedo, V., Rappenglueck, B., Cuchiara, G., Flynn, J., Ferrare, R., Scarino, A. J., et al. (2019). Bay breeze and sea breeze circulation impacts on the planetary boundary layer and air quality from an observed and modeled DISCOVER-AQ TX case study. *Journal of Geophysical Research: Atmospheres*, 124(13), 7359–7378. <https://doi.org/10.1029/2019JD030523>
- Changnon, S. A., Huff, F. A., & Semonin, R. G. (1971). METROMEX: An investigation of inadvertent weather modification. *Bulletin America Meteorology Social*, 52(10), 958–968. [https://doi.org/10.1175/1520-0477\(1971\)052<0958:MAOIW>2.0.CO;2](https://doi.org/10.1175/1520-0477(1971)052<0958:MAOIW>2.0.CO;2)
- Chen, F., Miao, S., Tewari, M., Bao, J. W., & Kusaka, H. (2011). A numerical study of interactions between surface forcing and sea breeze circulations and their effects on stagnation in the greater Houston area. *Journal of Geophysical Research*, 116(D12), 1–19. <https://doi.org/10.1029/2010JD015533>
- Ching, J., Brown, M., Burian, S., Chen, F., Cionco, R., Hanna, A., et al. (2009). National urban database and access portal tool. *Bulletin America Meteorology Social*, 90(8), 1157–1168. <https://doi.org/10.1175/2009BAMS2675.1>
- Ching, J., Mills, G., Bechtel, B., See, L., Feddema, J., Wang, X., et al. (2018). WUDAPT: An urban weather, climate, and environmental modeling infrastructure for the anthropocene. *Bulletin America Meteorology Social*, 99(9), 1907–1924. <https://doi.org/10.1175/BAMS-D-16-0236.1>
- Chiu, C. T. F., Wang, K., Paschalidis, A., Erfani, T., Peleg, N., Fatichi, S., et al. (2022). An analytical approximation of urban heat and dry islands and their impact on convection triggering. *Urban Climate*, 46, 101346. <https://doi.org/10.1016/j.uclim.2022.101346>
- Crosman, E. T., & Horel, J. D. (2012). Idealized large-eddy simulations of sea and lake breezes: Sensitivity to lake diameter, heat flux and stability. *Boundary-Layer Meteorology*, 144(3), 309–328. <https://doi.org/10.1007/s10546-012-9721-x>
- Demuzere, M., Argüeso, D., Zonato, A., & Kittner, J. (2022). W2W: A Python package that injects WUDAPT's local climate zone information in WRF. *Journal of Open Source Software*, 7(76), 4432. <https://doi.org/10.21105/joss.04432>
- Demuzere, M., He, C., Martilli, A., & Zonato, A. (2023). A hybrid 100-m global land cover dataset with Local Climate Zones for WRF [Dataset]. *Zenodo*. <https://doi.org/10.5281/zenodo.7670653>
- Demuzere, M., Kittner, J., & Bechtel, B. (2021). LCZ generator: A web application to create local climate zone maps. *Frontiers in Environmental Science*, 9. <https://doi.org/10.3389/fenvs.2021.637455>
- Demuzere, M., Kittner, J., Martilli, A., Mills, G., Moede, C., Stewart, I. D., et al. (2022). A global map of Local Climate Zones to support earth system modelling and urban scale environmental science. *Earth System Science Data*, 14(8), 3835–3873. <https://doi.org/10.5194/essd-14-3835-2022>
- Doan, Q., Kobayashi, S., Kusaka, H., Chen, F., He, C., & Niyogi, D. (2023). Tracking urban footprint on extreme precipitation in an African megacity. *Journal of Applied Meteorology and Climatology*, 62(2), 209–226. <https://doi.org/10.1175/JAMC-D-22-0048.1>
- Ebi, K. L., Capon, A., Berry, P., Broderick, C., de Dear, R., Havenith, G., et al. (2021). Hot weather and heat extremes: Health risks. *The Lancet*, 398(10301), 698–708. [https://doi.org/10.1016/S0140-6736\(21\)01208-3](https://doi.org/10.1016/S0140-6736(21)01208-3)
- Fan, J., Zhang, Y., Li, Z., Hu, J., & Rosenfeld, D. (2020). Urbanization-induced land and aerosol impacts on sea-breeze circulation and convective precipitation. *Atmospheric Chemistry and Physics*, 20(22), 14163–14182. <https://doi.org/10.5194/acp-20-14163-2020>
- Fan, Y. F., Li, Y. G., Bejan, A., Wang, Y., & Yang, X. Y. (2017). Horizontal extent of the urban heat dome flow. *Scientific Reports*, 7(1), 11681. <https://doi.org/10.1038/s41598-017-09917-4>
- Fischer, E., & Schär, C. (2010). Consistent geographical patterns of changes in high-impact European heatwaves. *Nature Geoscience*, 3(6), 398–403. <https://doi.org/10.1038/ngeo866>
- Guo, Y., Gasparini, A., Li, S., Sera, F., Vicedo-Cabrera, A. M., de Sousa Zanotti Staglorio Coelho, M., et al. (2018). Quantifying excess deaths related to heatwaves under climate change scenarios: A multicountry time series modelling study. *PLoS Medicine*, 15(7), e1002629. <https://doi.org/10.1371/journal.pmed.1002629>
- Han, L., Wang, L., Chen, H., Xu, Y., Sun, F., Reed, K., et al. (2022). Impacts of long-term urbanization on summer rainfall climatology in Yangtze River Delta agglomeration of China. *Geophysical Research Letters*, 49(13), e2021GL097546. <https://doi.org/10.1029/2021GL097546>
- Hawbecker, P., & Knivvel, J. C. (2022). Simulating the Chesapeake Bay Breeze: Sensitivities to water surface temperature. *Journal of Applied Meteorology and Climatology*, 61(11), 1595–1611. <https://doi.org/10.1175/JAMC-D-22-0002.1>

- Hendricks, E. A., Knievel, J. C., & Wang, Y. (2020). Addition of multilayer urban canopy models to a nonlocal planetary boundary layer parameterization and evaluation using ideal and real cases. *Journal of Applied Meteorology and Climatology*, 59(8), 1369–1392. <https://doi.org/10.1175/jamc-d-19-0142.1>
- Houston Climate Action Plan. (2020). Retrieved from <http://greenhoustonx.gov/climateactionplan/>
- Hu, Y. H., Hou, M. T., Jia, G. S., Zhao, C. L., Zhen, X. J., & Xu, Y. H. (2019). Comparison of surface and canopy urban heat islands within megacities of eastern China. *ISPRS Journal of Photogrammetry and Remote Sensing*, 156, 160–168. <https://doi.org/10.1016/j.isprsjprs.2019.08.012>
- Jensen, M. P., Flynn, J. H., Judd, L. M., Kollias, P., Kuang, C., Mcfarquhar, G., et al. (2022). A succession of cloud, precipitation, aerosol, and air quality field experiments in the coastal urban environment. *Bulletin America Meteorology Social*, 103(2), 103–105. <https://doi.org/10.1175/bams-d-21-0104.1>
- Jin, L., Schubert, S., Fenner, D., Meier, F., & Schneider, C. (2021). Integration of a building energy model in an urban climate model and its application. *Boundary-Layer Meteorology*, 178(2), 249–281. <https://doi.org/10.1007/s10546-020-00569-y>
- Kim, Y., Sartelet, K., Raut, J.-C., & Chazette, P. (2013). Evaluation of the weather research and forecast/urban model over greater Paris. *Boundary-Layer Meteorology*, 149(1), 105–132. <https://doi.org/10.1007/s10546-013-9838-6>
- Knievel, J. C., Bryan, G. H., & Hacker, J. P. (2007). Explicit numerical diffusion in the WRF model. *Monthly Weather Review*, 135(11), 3808–3824. <https://doi.org/10.1175/2007mwr2100.1>
- Krayenhoff, E., Broadbent, A., Zhao, L., Georgescu, M., Middel, A., Voogt, J., et al. (2021). Cooling hot cities: A systematic and critical review of the numerical modelling literature. *Environmental Research Letters*, 16(5), 053007. <https://doi.org/10.1088/1748-9326/abdcf1>
- Li, Q., Yang, J., & Yang, L. (2021). Impact of urban roughness representation on regional hydrometeorology: An idealized study. *Journal of Geophysical Research: Atmospheres*, 126(4), e2020JD033812. <https://doi.org/10.1029/2020jd033812>
- Lorenz, J. M., Kronenberg, R., Bernhofer, C., & Niyogi, D. (2019). Urban rainfall modification: Observational climatology over Berlin, Germany. *Journal of Geophysical Research: Atmospheres*, 124(2), 731–746. <https://doi.org/10.1029/2018JD028858>
- Loughner, C. P., Allen, D. J., Pickering, K. E., Dickerson, R. R., Zhang, D.-L., & Shou, Y.-X. (2011). Impact of the Chesapeake Bay breeze and fair-weather cumulus clouds on pollutant transport and transformation. *Atmospheric Environment*, 24, 4060–4072.
- Moraglia, G., Pryor, S. C., & Crippa, P. (2024). Quantifying the impacts of an urban area on clouds and precipitation patterns: A modeling perspective. *Journal of Geophysical Research: Atmospheres*, 129(12), e2024JD041402. <https://doi.org/10.1029/2024JD041402>
- Morris, C. J. G., Simmonds, I., & Plummer, N. (2001). Quantification of the influences of wind and cloud on the nocturnal urban heat island of a large city. *Journal of Applied Meteorology*, 40(2), 169–182. [https://doi.org/10.1175/1520-0450\(2001\)040<0169:qotio>2.0.co;2](https://doi.org/10.1175/1520-0450(2001)040<0169:qotio>2.0.co;2)
- National Centers for Environmental Prediction/National Weather Service/NOAA/U.S. Department of Commerce. (2015). Updated daily. NCEP GDAS/FNL 0.25 degree global tropospheric analyses and Forecast grids. *Research Data Archive at the National Center for Atmospheric Research, Computational and Information Systems Laboratory*. <https://doi.org/10.5065/D65Q4T4Z>
- Ngan, F., Kim, H., Lee, P., Al-Wali, K., & Dornblaser, B. (2013). A study of nocturnal surface wind speed overprediction by the WRF-ARW model in southeastern Texas. *Journal of Applied Meteorology and Climatology*, 52(12), 2638–2653. <https://doi.org/10.1175/JAMC-D-13-060.1>
- Oke, T. R. (1982). The energetic basis of the urban heat island. *The Quarterly Journal of the Royal Meteorological Society*, 108(455), 1–24. <https://doi.org/10.1002/qj.49710845502>
- Oliveira, A. P., Bornstein, R. D., & Soares, J. (2003). Annual and diurnal wind patterns in the city of São Paulo. *Water, Air, and Soil Pollution: Focus*, 3(5/6), 3–15. <https://doi.org/10.1023/A:1026090103764>
- Palecki, M., Durre, I., Applequist, S., Arguez, A., & Lawrimore, J. (2021). *U.S. Climate Normals 2020: U.S. Climate Normals (1991–2020)*. HOUSTON NWSO, TX (station ID: USC0041433). NOAA National Centers for Environmental Information. Retrieved from <https://www.ncdc.noaa.gov/>
- Peng, S., Piao, S., Ciais, P., Friedlingstein, P., Ottle, C., Bréon, F. M., et al. (2012). Surface urban heat island across 419 global big cities. *Environmental Science & Technology*, 46(2), 696–703. <https://doi.org/10.1021/es2030438>
- Powers, J. G., & Coauthors (2017). The weather research and forecasting model: Overview, system efforts, and future directions. *Bulletin America Meteorology Social*, 98, 1717–1737. <https://doi.org/10.1175/BAMS-D-15-00308.1>
- Pu, B., & Dickinson, R. E. (2014). Diurnal spatial variability of Great Plains summer precipitation related to the dynamics of the low-level Jet. *Journal of the Atmospheric Sciences*, 71(5), 1807–1817. <https://doi.org/10.1175/JAS-D-13-0243.1>
- Qian, Y., Chakraborty, T. C., Li, J., Li, D., He, C., Sarangi, C., et al. (2022). Urbanization impact on regional climate and extreme weather: Current understanding, uncertainties, and future research directions. *Advances in Atmospheric Sciences*, 39(6), 819–860. <https://doi.org/10.1007/s00376-021-1371-9>
- Rahman, K., Rios, G., Gamarro, H., Addasi, O., Peña, J. C., Gonzalez-Cruz, J., et al. (2024). The boundary layer characteristics of coastal urban environments. *Theoretical and Applied Climatology*, 155(7), 6931–6948. <https://doi.org/10.1007/s00704-024-05036-z>
- Resilient Houston. (2020). Retrieved from <https://www.houstonx.gov/mayor/Resilient-Houston-20200518-single-page.pdf>
- Rosenzweig, C., Horton, R. M., Bader, D. A., Brown, M. E., DeYoung, R., Dominguez, O., et al. (2014). Enhancing climate resilience at NASA Centers: A collaboration between science and Stewardship. *Bulletin America Meteorology Social*, 95(9), 1351–1363. <https://doi.org/10.1175/bams-d-12-00169.1>
- Rothfuss, L. P. (1990). The heat index “equation” (or, more than you ever wanted to know about heat index). *NWS Tech. Attachment SR*, 90–23, 2.
- Ryu, Y., Smith, J. A., Bou-Zeid, E., & Baeck, M. L. (2016). The influence of land surface heterogeneities on heavy convective rainfall in the Baltimore–Washington metropolitan area. *Monthly Weather Review*, 144(2), 553–573. <https://doi.org/10.1175/MWR-D-15-0192.1>
- Salamanca, F., Martilli, A., Tewari, M., & Chen, F. (2011). A study of the urban boundary layer using different urban parameterizations and high-resolution urban canopy parameters with WRF. *Journal of Applied Meteorology and Climatology*, 50(5), 1107–1128. <https://doi.org/10.1175/2010JAMC2538.1>
- Salas-Monreal, D., Anis, A., & Alberto Salas-de-Leon, D. (2018). Galveston Bay dynamics under different wind conditions. *Oceanologia*, 60(2), 232–243. <https://doi.org/10.1016/j.oceano.2017.10.005>
- Schubert, S., Grossman-Clarke, S., & Martilli, A. (2012). A double-canyon radiation scheme for multi-layer urban canopy models. *Boundary-Layer Meteorology*, 145(3), 439–468. <https://doi.org/10.1007/s10546-012-9728-3>
- Seigel, R. B. (2014). Shallow cumulus mixing and subcloud-layer responses to variations in aerosol loading. *Journal of the Atmospheric Sciences*, 71(7), 2581–2603. <https://doi.org/10.1175/JAS-D-13-0352.1>
- Shem, W., & Shepherd, M. (2009). On the impact of urbanization on summertime thunderstorms in Atlanta: Two numerical model case studies. *Atmospheric Research*, 92(2), 172–189. <https://doi.org/10.1016/j.atmosres.2008.09.013>
- Shen, L. D., Sun, J. N., & Yuan, R. M. (2018). Idealized large eddy simulation study of interaction between urban heat island and sea breeze circulations. *Atmospheric Research*, 214, 338–347. <https://doi.org/10.1016/j.atmosres.2018.08.010>

- Simolo, C., Brunetti, M., Maugeri, M., & Nanni, T. (2011). Evolution of extreme temperatures in a warming climate. *Geophysical Research Letters*, 38(16), L16701. <https://doi.org/10.1029/2011GL048437>
- Spangler, T. C., & Dirks, R. A. (1974). Meso-scale variations of the urban mixing height. *Boundary-Layer Meteorology*, 6(3–4), 423–441. <https://doi.org/10.1007/BF02137677>
- Statkewicz, M. D., & Rappenglueck, B. (2023). A comparative analysis of the sea breeze on the Texas Gulf Coast and its impact on precipitation. *Urban Climate*, 49, 101568. <https://doi.org/10.1016/j.ulclim.2023.101568>
- Statkewicz, M. D., Talbot, R., & Rappenglueck, B. (2021). Changes in precipitation patterns in Houston, Texas. *Environmental Advances*, 5, 100073. <https://doi.org/10.1016/j.envadv.2021.100073>
- Theeuwes, N. E., Barlow, J. F., Teuling, A. J., Grimmond, C. S. B., & Kotthaus, S. (2019). Persistent cloud cover over mega-cities linked to surface heat release. *npj Climate and Atmospheric Science*, 2(1), 15. <https://doi.org/10.1038/s41612-019-0072-x>
- Theeuwes, N. E., Boutle, I. A., Clark, P. A., & Grimmond, S. (2021). Understanding London's summertime cloud cover. *Quarterly Journal of the Royal Meteorological Society*, 148(742), 454–465. <https://doi.org/10.1002/qj.4214>
- Trenberth, K., Fasullo, J., & Shepherd, T. (2015). Attribution of climate extreme events. *Nature Climate Change*, 5(8), 725–730. <https://doi.org/10.1038/nclimate2657>
- USGCRP. (2018). In D. R. Reidmiller, C. W. Avery, D. R. Easterling, K. E. Kunkel, K. L. M. Lewis, et al. (Eds.), *Impacts, risks, and adaptation in the United States: Fourth national climate assessment* (Vol. II, p. 1515). U.S. Global Change Research Program. <https://doi.org/10.7930/NCA4.2018>
- Venter, Z. S., Chakraborty, T., & Lee, X. (2021). Crowdsourced air temperatures contrast satellite measures of the urban heat island and its mechanisms. *Science Advances*, 7(22), eabb9569. <https://doi.org/10.1126/sciadv.eabb9569>
- Vo, T. T., Hu, L., Xue, L., Li, Q., & Chen, S. (2023). Urban effects on local cloud patterns. *Proceedings of the National Academy of Sciences of the United States of America*, 120(21), e2216765120. <https://doi.org/10.1073/pnas.2216765120>
- Wang, D., Jensen, M. P., Taylor, D., Kowalski, G., Hogan, M., Wittemann, B. M., et al. (2022). Linking synoptic patterns to cloud properties and local circulations over southeastern Texas. *Journal of Geophysical Research: Atmospheres*, 127(5), e2021JD035920. <https://doi.org/10.1029/2021JD035920>
- Wang, J., Qian, Y., Pringle, W., Chakraborty, T. C., Hetland, R., Yang, Z., & Xue, P. (2023). Contrasting effects of lake breeze and urbanization on heat stress in Chicago metropolitan area. *Urban Climate*, 48, 101429. <https://doi.org/10.1016/j.ulclim.2023.101429>
- Williams, A. P., Schwartz, R. E., Iacobellis, S., Seager, R., Cook, B. I., Still, C. J., et al. (2015). Urbanization causes increased cloud base height and decreased fog in coastal Southern California. *Geophysical Research Letters*, 42(5), 1527–1536. <https://doi.org/10.1002/2015GL063266>
- Wilson, A. M., & Jetz, W. (2016). Remotely sensed high-resolution global cloud dynamics for predicting ecosystem and biodiversity distributions. *PLoS Biology*, 14(3), e1002415. <https://doi.org/10.1371/journal.pbio.1002415>
- WMO. (2008). *Guide to meteorological instruments and methods of observation*. World Meteorological Organization.
- Zhong, S., Qian, Y., Zhao, C., Leung, R., Wang, H., Yang, B., et al. (2017). Urbanization-induced urban heat island and aerosol effects on climate extremes in the Yangtze River Delta region of China. *Atmospheric Chemistry and Physics*, 17(8), 5439–5457. <https://doi.org/10.5194/acp-17-5439-2017>
- Zhong, S., Qian, Y., Zhao, C., Leung, R., & Yang, X. Q. (2015). A case study of urbanization impact on summer precipitation in the Greater Beijing Metropolitan Area: Urban heat island versus aerosol effects. *J. Geophys. Res.-Atmos.*, 120(20), 10903–10914. <https://doi.org/10.1002/2015jd023753>
- Zhu, X., Ni, G., Cong, Z., Sun, T., & Li, D. (2016). Impacts of surface heterogeneity on dry planetary boundary layers in an urban-rural setting. *Journal of Geophysical Research: Atmospheres*, 121(20), 12164–12179. <https://doi.org/10.1002/2016JD024982>
- Zonato, A., Martilli, A., Gutierrez, E., Chen, F., He, C., Barlage, M., et al. (2021). Exploring the effects of rooftop mitigation strategies on urban temperatures and energy consumption. *Journal of Geophysical Research: Atmospheres*, 126(21), e2021JD035002. <https://doi.org/10.1029/2021JD035002>